LOCALIZATION OF EMITTERS OVER AND AROUND SEA SURFACES

A MASTER'S THESIS

in

Electrical and Electronics Engineering

Atılım University

by

YASER DALVEREN

JULY 2011

LOCALIZATION OF EMITTERS OVER AND AROUND SEA SURFACES

A THESIS SUBMITTED TO

THE GRADUATE SCHOOL OF NATURAL AND APPLIED SCIENCES

OF

ATILIM UNIVERSITY

BY

YASER DALVEREN

IN PARTIAL FULFILLMENT OF THE REQUIREMENTS FOR THE DEGREE OF

MASTER OF SCIENCE

IN

THE DEPARTMENT OF ELECTRICAL AND ELECTRONICS ENGINEERING

JULY 2011

Approval of the Graduate School of Natural and Applied Sciences, Atılım University.

_____

Prof. Dr. İbrahim Akman

Director

I certify that this thesis satisfies all the requirements as a thesis for the degree of Master of Science.

_____

Assoc. Prof. Dr. Elif Uray Aydın

Head of Department

This is to certify that we have read the thesis "Localization of Emitters Over and Around Sea Surfaces" submitted by "Yaser Dalveren" and that in our opinion it is fully adequate, in scope and quality, as a thesis for the degree of Master of Science.

_____

Assoc. Prof. Dr. Ali Kara

Supervisor

Examining Committee Members

Assoc. Prof. Dr. Elif Uray AYDIN _____

Assoc. Prof. Dr. Ali KARA _____

Assoc. Prof. Dr. Bülent TAVLI _____

Asst. Prof. Dr. Nergiz ÇAĞILTAY _____

Asst. Prof. Dr. Mehmet Efe ÖZBEK _____

Date: 21.07.2011

I declare and guarantee that all data, knowledge and information in this document has been obtained, processed and presented in accordance with academic rules and ethical conduct. Based on these rules and conduct, I have fully cited and referenced all material and results that are not original to this work.

Name, Last name: Yaser Dalveren

Signature:

ABSTRACT

LOCALIZATION OF EMITTERS OVER AND AROUND SEA SURFACES

Dalveren, Yaser

M.S., Electrical and Electronics Engineering Department

Supervisor: Assoc. Prof. Dr. Ali Kara

July 2011, 70 pages

This thesis presents an approach for localization of emitters over and around the sea by using passive scatterers and Geographic Information System (GIS). Multipath propagation model involves three-rays consisting of line-of-sight (LOS) propagation and two reflected propagation paths. For these conditions, a direct and short derivation of an algorithm based on the closed-form solution of the nonlinear equations for emitter localization using Time Difference of Arrival (TDOA) between the rays is proposed. The thesis also discusses Electromagnetic (EM) modeling and classification of scatterers over and around sea for localization problem. In this context, bistatic scattering properties of some known objects are analyzed and measured scattering coefficients are collected from the literature. According to gathered scattering coefficients, data table is provided to make classification of passive scatterers. Furthermore, performance of presented approach for localization is simulated under various conditions. Measurement error is also addressed and system performance is discussed shortly.

Keywords: Time Difference of Arrival, Emitter Localization, Radar Cross Sections, Bistatic Scattering

ÖZ

DENİZ YÜZEYİ ÇEVRESİNDEKİ EMİTÖRLERİN LOKASYON TESPİTİ

Dalveren, Yaser

Yüksek Lisans, Elektrik-Elektronik Mühendisliği Bölümü

Tez Yöneticisi: Doç. Dr. Ali Kara

Temmuz 2011, 70 sayfa

Bu tez, pasif yansıtıcılar ve Coğrafi Bilgi Sistemi (CBS) kullanarak deniz üzerinde veya çevresinde bulunan emitörlerin yerini belirlemeyi amaçlamaktadır. Düşünülen çoklu yayılım modeli, görüş hattı ve iki yansımış yayılım hattı içeren üç ışımalı modeldir. Bu koşullarda, emitörün yerini belirlemek için, yayılım hatları arasındaki varış zaman farkı (VZF) ölçümleri kullanarak, sonlucu ifade çözümüne dayalı doğrusal olmayan denklemlerin çözüm algoritmasının direk ve kısa bir ispatı önerilmiştir. Çalışmada ayrıca, deniz üzerindeki ve çevresindeki yansıtıcıların, elektromanyetik modelleme ve sınıflandırılması da tartışmaktadır. Bu bağlamda, bilinen bazı yansıtıcıların bistatik yansıtma özellikleri analiz edilmekte ve yansıtma katsayıları literatür taraması ile bir araya getirilmektedir. Bir araya getirilen yansıtma katsayılarına göre, saçıcıları sınıflandırmak için veri tablosu sağlanmaktadır. Ayrıca, yer belirleme için verilen yaklaşımın benzetimi yapılmakta ve ölçüm hatasına yönelik basit analizler sunulmaktadır.

Anahtar Kelimeler: Varış Zaman Farkı, Konum Belirleme, Radar Kesit Alanı, Bistatik Saçılma

To My Family (Aileme)

ACKNOWLEDGMENTS

I would like to express my sincere thanks and gratitude to my supervisor Assoc. Prof. Dr. Ali Kara for his belief, encouragements, complete guidance, advice and criticism throughout this study.

To my mother, Aycan Dalveren, I offer sincere thanks for her continuous support and patience during this period.

TABLE OF CONTENTS

LIST OF TABLES

TABLE

LIST OF FIGURES

FIGURE

LIST OF ABBREVIATIONS

AOA	-	Angle of Arrival
EI	-	Electronic Intercept
EM	-	Electromagnetic
ESPRIT	-	Estimation of Signal Parameters via Rotational Invariance Techniques
FDOA	-	Frequency Difference of Arrival
GIS	-	Geographic Information System
LOS	-	Line of Sight
ML	-	Maximum Likelihood
MUSIC	-	Multiple Signal Classification
NRCS	-	Normalized Radar Cross Section
RCS	-	Radar Cross Section
RD	-	Range Difference
RS	-	Remote Sensing
TDOA	-	Time Difference of Arrival

CHAPTER 1

INTRODUCTION

Multipath propagation occurs when multiple copies of the transmitted signal arrive at the receiver from different paths. This results in multiple copies of the signal with different phase, magnitude and time of arrival. In bistatic cases, electromagnetic propagation from the transmitter to the receive antenna consists of a line-of-sight (LOS) propagation path and usually a number of multipath reflections. This thesis is mainly based on using time difference of arrival measurements (TDOA) via Geographical Information System (GIS) for determining emitter location over and around sea.

Emitter localization by TDOA has many applications in Electronic Intercept (EI) systems. In emitter localization by TDOA, the emitter is assumed to transmit a signal which is received by multiple receivers at known locations, and the TDOA values between signals received at pairs of receivers are utilized to determine the location of the emitter. The localization of an emitter by TDOA requires solving a set of nonlinear equations obtained from TDOA measurements and known receiver locations [1]. The existing solutions to this problem can be loosely divided into three categories:

i. Maximum likelihood (ML) estimator,

ii. Closed-form solutions with parameter constraints,

iii. Closed-form asymptote intersection estimator.

Since closed-form solutions with parameter constraints are achieved a good accuracy and usually less computationally burdensome than ML estimator and closed-form asymptote intersection estimator, solution of the nonlinear equations for emitter location using TDOA measurements is considered [2].

When an object is placed in the beam of a radar, it disperses some of the incident energy in all directions. This dispersal is called scattering, a term borrowed from physics, and the resulting field distribution in space depends on the size, shape, and composition of the object and on the waveform and direction of arrival of the incident wave. The spatial distribution of the scattered energy can be described in terms of a Radar Cross Section (RCS) and the object itself are often called scatterers. This general distribution of the scattered field, to the exclusion of the incident field, is called bistatic scattering, implying all scattering directions where a finite angle is subtended by the direction of incidence and the direction of interest. It is probably natural and convenient to describe the echo characteristics of targets in the beam of a radar in terms of an area. For arbitrary directions, that area is known as the bistatic radar cross section [3].

The scattering properties of natural surfaces are commonly represented by the scattering coefficients. The scattering coefficient is the radar cross section per unit area of surface and it gives the RCS of a radar resolution cell when it is multiplied by the illuminated area.

Therefore, bistatic scattering coefficient measurements of some known objects may be necessary to analyze to make classification of scatterers. Hence, data collection of bistatic scattering measurements of some known objects over and around the sea is gathered after making literature survey [4-23]. According to these collected bistatic scattering coefficients, the data table is provided to make classification easier. This classification process could be used to identify candidate scatterers, which are chosen as virtual sensors, to be used in TDOA technique implemented later.

Intercept receivers must perform the tasks of detection, parameter identification, and classification in a complex environment of multiple signals. Modern operational

system needs increasingly require intercept systems. It implies not only more accurate emitter identification but also a very accurate passive emitter location. This study is proposed for emitter localization by passive scatterers that can be used an in intercept system. This system is also interested for scientists and engineers to estimate emitter location over and around sea by using arrival times of signals received by multiple passive scatterers.

This thesis begins with problem statement in Chapter 2. Considerations to generate a scenario for finding emitter location and classifying scatterers are discussed, too.

A comprehensive discussion on time difference of arrival methods is given in Chapter 3. Then, derivation of emitter location by using TDOA technique is provided.

Chapter 4 begins with definition of the RCS. After that, the terms of surface clutter and clutter radar cross sections are defined to understand bistatic scattering measurements better. Geometry of bistatic clutter measurements and angles which are related to these geometries are given. Finally, scatterers whose bistatic scattering coefficients are known in literature are determined.

Chapter 5 is divided into two main parts. First part introduces scatterer classification where various bistatic scattering measurements of scatterers are collected and analyzed from the open literature in Chapter 4, and then classification process is proposed. The generalized data table is made to classify the scatterers. The detailed data table is given in Appendix, too. Second part of Chapter 5 presents an algorithm to determine emitter location using TDOA technique. The existence of a solution is proved and some specific propositions to assumptions are provided. Implementation of proposed method for realistic environments is described. Simulation scenarios are given and performance comparison of the proposed method is presented under these scenarios. Measurement error is also addressed, and test results are discussed.

Finally, the conclusions are emphasized and future work is proposed in Chapter 6.

CHAPTER 2

PROBLEM STATEMENT

In this study, emitter localization by passive scatterers over the sea is considered. Considered system uses antennas at different locations for transmission and reception in two dimensional (2D) coordinate system. This is called "Bistatic Radar". The basic definition of bistatic radar is straightforward: a radar operating with separated transmitting and receiving antennas [24]. Presented approach for emitter localization has two components. One is measurement, or choice of sensors, and the other is estimation/information fusion, or processing of measurements provided by the sensors. Estimation of emitter location is basis on TDOA technique. In this technique, position of sensors are necessary, because the problem of estimating location of an emitter can be solved by processing relative arrival time differences at three or more sensors [25]. Pulse arrival times are measured by sensors in radar applications. In this method, one of the sensors is chosen as the reference and time difference of arrival of the pulses are expressed relative to the reference. This sensor is also assumed as a receiver. Thus, these measurements are called as TDOA and by using these TDOA measurements, a direct and short algorithm based on the closed - form solution of the nonlinear equation is provided for emitter localization, as to be discussed in Chapter 3. Given method in Chapter 3 represents a two-step solution. First, a quadratic equation, which is related to a set of nonlinear range difference equation, required to be solved to find the range from emitter to receiver, R_s and then, R_s is used as to determine the emitter position. Quadratic equation form of R_s can be expressed as

$$aR_s^2 + bR_s + c = 0 \tag{1}$$

where, a, b, and c are variables.

In some instances, (1) will permit two physical solutions. From the mathematics, the roots of (1) can be found by

$$R_s = \frac{-b \pm \sqrt{b^2 - 4ac}}{2a} \tag{2}$$

only the case of $R_s \geq 0$. To ensure the case of $R_s \geq 0$, following condition must be satisfied,

$$b^2 - 4ac \geq 0 \tag{3}$$

If condition (3) does not hold, then a real solution does not exist.

In these situations, the two locations are usually far enough apart. The correct solution can be discerned by other physical reasoning such as one solution lying outside the domain of interest. However, an existence of a solution is proposed in Chapter 5 to get unique, real and positive location solution to nonlinear equation (1). Herewith, component of estimation in emitter localization may be accomplished.

In EI systems, received digital signal are clustered according to Radio Frequency (RF), Angle of Arrival (AOA), and Pulse Width (PW) values. After checking the geography of the region via GIS, scatterers are decided from these signal clusters on the basis of scattering coefficients, σ^0. GIS is a system designed to capture, store, manipulate, analyze, manage and present all types of geographically referenced data. With the development of science and technology, computer technologies, especially remote sensing (RS) technology and GIS technology, play a dominant role in classification. Furthermore, in scatterer decision, a classification of objects over the sea is required. In order to make object classification, RCS of objects is necessary since calculation of the RCS of objects is one of the important subjects for object classifying as stated in Chapter 4. In radar applications, the electromagnetic power

intercepted by a target is modeled via a hypothetical area known as RCS. The power intercepted by the object is calculated as the product of RCS and the power density at the target location. However, the scattering properties of natural surfaces are commonly represented by the scattering coefficients. Then, scattering coefficients of objects over the sea is necessary to analyze. Detailed discussion is provided in Chapter 4 and classification table is given in Chapter 5. Therefore, scatterers, which have a good ability of scattering coefficient, are chosen as a candidate sensor by using GIS and given classification table. These virtual sensors are, then used in localization of the emitter. Thus, choice of sensor component in emitter localization may be achieved. Since receiver position is assumed at the origin, (0,0), new calculations are necessary for determining position of scatterers in 2D system. In this context, slant ranges from the sensors to the receiver are obtained by using satellite map. Then, from the geometry, using point – slope equation of a line is essential to determine new position of sensors. Discussion about these instructions is given in Chapter 5.

TDOA based localization is implemented in real environment to test its accuracy. Realistic scenarios are created and they are considered in Aegean Sea as can be seen in Chapter 5. Decision of scatterers is ignored and two islands are assumed as artificial scatterers. A short and efficient algorithm based on the closed-form solution as given in Chapter 3, is used for emitter localization over Aegean Sea. Time of arrival error is introduced to localization problem and emitter position is estimated with an error range. Terrain types of scatterers (islands) are also analyzed and classified according the provided classification table in Section 5.1.

CHAPTER 3

TIME DIFFERENCE OF ARRIVAL BASED LOCALIZATION

In EI systems, location of an emitter can be estimated by using TDOA, Angle of Arrival (AOA) and/or Frequency Difference of Arrival (FDOA) measurements, or any other localization technique. For example, high resolution direction finding methods such as amplitude comparison, phase comparison or subspace techniques like Multiple Signal Classification (MUSIC) or Estimation of Signal Parameters via Rotational Invariance Techniques (ESPRIT) can be applied [26].

On the other hand, these methods require proper antenna calibration which is not necessary with TDOA. This is one of the most important properties of TDOA. In addition, TDOA measurements are constructed by using arrival times of signals received by multiple passive sensors. Therefore, no knowledge about the waveform of the received signal is required. Because of these facts, emitter localization by TDOA is considered as one of the elegant localization methods and it is advantageous among other localization techniques [27]. However, TDOA location estimation methods require accurate time synchronization between the sensors.

In open literature, there are numerous works on emitter location finding algorithms that use TDOA techniques. In these techniques, the solution of the emitter location problem includes different approaches which are using estimation of TDOAs between all sensors: Iterative Least-Squares (ILS) [28,29] and Maximum Likelihood (ML) estimation [30]. Conventionally, emitter location is estimated from the intersection of a set of hyperboloids defined by the Range Difference (RD) measurements. Accurate position location estimation of an emitter requires an

efficient hyperbolic position location estimation algorithm. Methods that are cited in [30] and [31], have been proposed for position location estimation based on TDOA technique.

Closed-form estimators can be seen to be as the most studied topic. Closed - form solutions [32,33] are using "spherical intersection" and "spherical interpolation" methods. To sum up, it can be said that closed - form solutions are usually less computationally burdensome than iterative, nonlinear minimization, or the ML method, and achieve good accuracy. In this chapter, a simple derivation of a closed-form solution is given [2].

Proposed method for emitter localization is accomplished in two stages [34]. The first stage, as provided in this chapter, involves estimation of the TDOA between sensors through the use of time delay estimation techniques. The estimated TDOAs are then transformed into range difference measurements between sensors, resulting in a set of nonlinear range difference equations. The second stage utilizes efficient algorithms to produce an unambiguous solution to the nonlinear equations. The exact solution is produced by these algorithms results in the estimated position location of the emitter. True TDOA is directly proportional to the difference in distance between the emitter (E) and the sensors (S_1 and S_2). A typical geometry is illustrated in Figure 1.

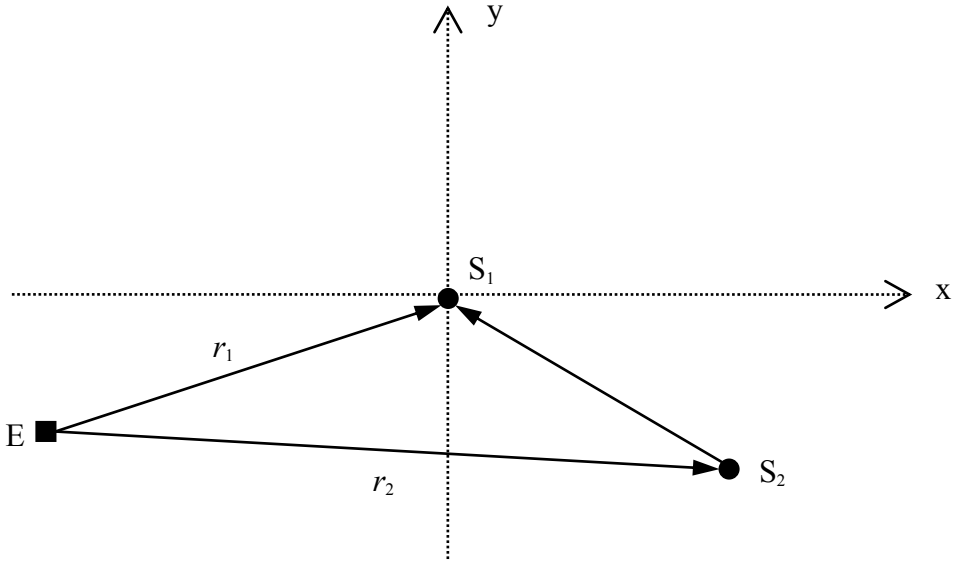

Figure 1 – TDOA Geometry

According to Figure 1, since the transmitter and/or the receiving systems can be elevated from the ground, r_1 are r_2 represent slant ranges between the emitter and the sensor systems.

These distances can be expressed as

$$r_i = ct_i, \quad i = 1,2 \tag{4}$$

where, c is the speed of light and t_i is the time that the signal arrives at the ith sensor.

TDOAs are directly proportional to the difference in distance between the emitter and the sensors, called range differences (RDs).

$$\tau = \Delta t_{1,2} = \Delta r_{1,2} / c = (r_1 - r_2) / c \tag{5}$$

where, τ is the time difference between the direct signal and scattered signal from the sensor.

A technique that yields the emitter localization in closed - form using TDOA is proposed [2]. In this chapter, a simple derivation of a closed - form solution [2] similar to [1] is given. This provides a direct and short derivation of the closed - form solution-based emitter localization algorithm. In general case, an estimate requires at least $N + 1$ sensors for N dimensional location estimate. To obtain a two dimensional (2D) emitter location solution, location of a minimum of three sensors are required to be known. As shown in Figure 2, one of the sensors is used as the reference sensor (S_0) for the RD measurements and this is usually placed at the origin of the coordinates system (x_0,y_0). Unknown emitter position (E) is also given as (x_s,y_s). Other sensors are defined as (x_1,y_1) and (x_2,y_2).

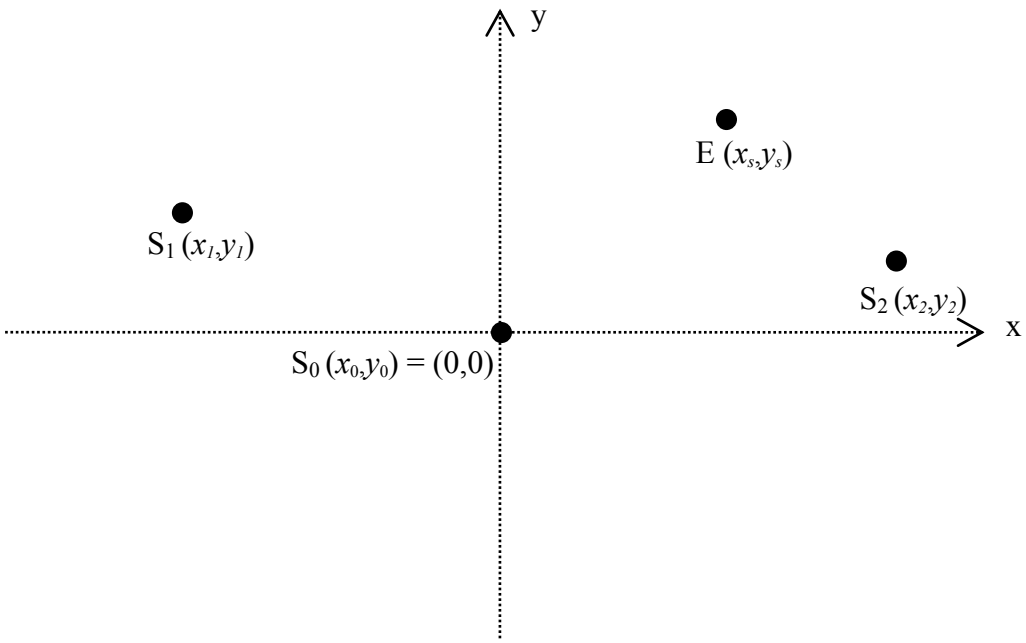

Figure 2 – Sensor Grid and Target in Two Dimensions

Emitter location can be determined by using the time differences at sensors with respect to reference sensor. The two TDOAs can be expressed as

$$\Delta t_i = t_i - t_0 \qquad i = 1,2 \tag{6}$$

where t_0 is the time of arrival to the reference sensor.

The TDOAs can be converted to RDs:

$$d_i = c\Delta t_i = c(t_i - t_0) \qquad i = 1,2 \tag{7}$$

Thus d_i is the RD between the reference and the *i*th sensor.

The coordinates of the sensors can be written as a vector form,

$$\mathbf{S_0} = \begin{bmatrix} x_0 \\ y_0 \end{bmatrix} = \begin{bmatrix} 0 \\ 0 \end{bmatrix} \tag{8}$$

and

$$\mathbf{S_i} = \begin{bmatrix} x_i \\ y_i \end{bmatrix} \qquad i = 0,1,2 \tag{9}$$

where, (x_0, y_0) is the reference sensor position, (x_i, y_i) is the *i*th sensor position.

The unknown emitter position is a vector form

$$\mathbf{E} = \begin{bmatrix} x_s \\ y_s \end{bmatrix} \tag{10}$$

The Euclidian distance between the emitter and sensor *i* (norm of the difference vector) is

$$R_{is} = \|\mathbf{S_i} - \mathbf{E}\| = \sqrt{(x_i - x_s)^2 + (y_i - y_s)^2} \qquad i = 1,2 \tag{11}$$

and the distance to the emitter

$$R_s = \| \mathbf{E} \| = \sqrt{x_s^{\,2} + y_s^{\,2}} \tag{12}$$

The RDs satisfy the basic relationships after using the RD notation d_i of (7):

$$d_i = R_{is} - R_s \qquad i = 1,2 \tag{13}$$

which can be rewritten using (11) and (12) as

$$d_i = \sqrt{(x_i - x_s)^2 + (y_i - y_s)^2} - \sqrt{x_s^{\,2} + y_s^{\,2}} \qquad i = 1,2 \tag{14}$$

After algebraic manipulation, (14) yields

$$x_i x_s + y_i y_s + d_i \sqrt{x_s^{\,2} + y_s^{\,2}} = \frac{1}{2}(x_i^2 + y_i^2 - d_i^2) \;\; i = 1, 2 \tag{15}$$

For the general case of 2 sensors, define the regressor matrix

$$\mathbf{S} = \begin{bmatrix} x_1 & y_1 \\ x_2 & y_2 \end{bmatrix}_{2x2} \tag{16}$$

Regressor matrix is defined to measure the extent to which a dependent variable $(\mathbf{S})$ is associated with one or more independent variables (sensor positions) as (x_1, y_1) and (x_2, y_2).

From the (15), vectors are defined as,

$$\mathbf{z} = \frac{1}{2}\begin{bmatrix} x_1^2 + y_1^2 - d_1^2 \\ x_2^2 + y_2^2 - d_2^2 \end{bmatrix}_{2x1} \tag{17}$$

and

$$\mathbf{d} = \begin{bmatrix} d_1 \\ d_2 \end{bmatrix}_{2x1} \tag{18}$$

In matrix notation, for multiple sensors (15) becomes

$$\mathbf{SE} = \mathbf{z} - \mathbf{d}Rs \tag{19}$$

Equation (19) represent a linear system with the three unknowns: x_s, y_s, and R_s. Hence, by solving (19) for emitter position **E**, the preliminary emitter position estimation is obtained as

$$\mathbf{E} = (\mathbf{S}^{\mathrm{T}}\mathbf{S})^{-1}\mathbf{S}^{\mathrm{T}}(\mathbf{z} - \mathbf{d}Rs) \tag{20}$$

$$\mathbf{E} = (\mathbf{S}^{\mathrm{T}}\mathbf{S})^{-1}\mathbf{S}^{\mathrm{T}}\mathbf{z} - (\mathbf{S}^{\mathrm{T}}\mathbf{S})^{-1}\mathbf{S}^{\mathrm{T}}\mathbf{d}Rs\,. \tag{21}$$

When not all RDs are measured to the same accuracy, a weighting matrix W_{2x2} is in order, in which case the preliminary emitter position estimate is

$$\hat{\mathbf{E}} = (\mathbf{S}^{\mathrm{T}}\mathbf{W}^{-1}\mathbf{S})^{-1}\mathbf{S}^{\mathrm{T}}\mathbf{W}^{-1}\mathbf{z} - (\mathbf{S}^{\mathrm{T}}\mathbf{W}^{-1}\mathbf{S})^{-1}\mathbf{S}^{\mathrm{T}}\mathbf{W}^{-1}\mathbf{d}Rs \tag{22}$$

A weighting matrix, W, is a matrix

$$W = \begin{bmatrix} M_{1A} & M_{1C} & M_{1G} & M_{1T} \\ M_{2A} & M_{2C} & M_{2G} & M_{2T} \\ \vdots & \vdots & \vdots & \vdots \\ M_{lA} & M_{lC} & M_{lG} & M_{lT} \end{bmatrix} \tag{23}$$

where l is the length of W, and $W[i,\alpha] = M_{i\alpha}$ is the number of occurrences of base α at position i. Let W_i be the total number of bases at a given position.

$$W_i = \sum_{\alpha \in A,C,G,T} M_{i\alpha} \tag{24}$$

If some observations are more important or more accurate than others, then different weights might be associated with different observations. Therefore, if it is desired to weight the RD's according to a priori confidence in each RD, then the weighting matrix can be created. It means, when the range (time of arrival) error is introduced

to system, receiver to sensor range can be weighted by the weighting matrix. For example,

if RDs from three sensors to receiver is known a priori confident, weighting matrix will be created as

$$W = \begin{bmatrix} 1 & 0 & 0 \\ 0 & 1 & 0 \\ 0 & 0 & 1 \end{bmatrix} \tag{25}$$

If the range between one of the sensor and receiver is not known priori, W might be expressed as

$$W = \begin{bmatrix} 1 & 0 & 0 \\ 0 & 1 & 0 \\ 0 & 0 & 0.2 \end{bmatrix} \tag{26}$$

However, as discussed in Chapter 5, it is not necessary to change the parameters in weighting matrix, since two scatterers are are chosen as virtual sensors for testing accuracy of emitter localization and 20% of time of arrival measurement (range) error is already introduced. Created weighting matrix is therefore basically based on simply diagonal and positive definite as given in (25) but represented by dimension of 2x2 since two sensor exist.

Then, defining new vectors from (22) as

$$\mathbf{a} = (\mathbf{S}^{\mathrm{T}}\mathbf{W}^{-1}\mathbf{S})^{-1}\mathbf{S}^{\mathrm{T}}\mathbf{W}^{-1}\mathbf{z} = \begin{bmatrix} a_1 \\ a_2 \end{bmatrix} \tag{27}$$

and

$$\mathbf{b} = (\mathbf{S}^{\mathrm{T}}\mathbf{W}^{-1}\mathbf{S})^{-1}\mathbf{S}^{\mathrm{T}}\mathbf{W}^{-1}\mathbf{d} = \begin{bmatrix} b_1 \\ b_2 \end{bmatrix} \tag{28}$$

(22) becomes

$$\hat{\mathbf{E}} = \mathbf{a} - \mathbf{b}R_s \tag{29}$$

Using the definitions (27) and (28), and (29), the following relationship holds:

$$\mathbf{E} = \begin{bmatrix} x_s \\ y_s \end{bmatrix} = \begin{bmatrix} a_1 - b_1 R_s \\ a_2 - b_2 R_s \end{bmatrix} \tag{30}$$

Inserting (30) into (13) and applying algebraic manipulations, yields the following quadratic equation for R_s;

$$(b_1^2 + b_2^2 - 1)R_s{}^2 - 2R_s(a_1 b_1 + a_2 b_2) + a_1^2 + a_2^2 = 0 \tag{31}$$

which has two solutions given by

$$\hat{R}_s = \frac{a_1 b_1 + a_2 b_2 \pm \sqrt{(a_1 b_1 + a_2 b_2)^2 + (b_1^2 + b_2^2 - 1)(a_1^2 + a_2^2)}}{b_1^2 + b_2^2 - 1} \tag{32}$$

The solutions to (32) are used as the solution to the estimated emitter to reference sensor distance $\hat{R}_s$. Substituting this value for $\hat{R}_s$ into (29) finally yields the estimated signal emitter location $\hat{\mathbf{E}}$. Thus, both minus and plus signs are applied two estimated emitter positions. From the (32), two results are ensued, so other information must be used to determine exact position of the emitter. In order to get exact position, an existence of a solution is required to degrade two real emitter positions to a unique position. Discussion about the existence of a solution is provided in Section 5.2.

After giving some cases to degrade two real emitter positions to a unique, real and positive position, provided approach for emitter localization is implemented to real scenarios in Section 5.2. In these scenarios, receiver is placed at the origin since it is assumed as a reference sensor. Two artificial scatterers over sea, such as islands, are chosen as virtual sensors. For emitter localization over sea, first (32) is solved to determine the distance of emitter to receiver. Next, provided unique R_s value, as founded by using existence of a solution, is substituted into (29) for emitter localization. Detailed discussion is provided in Section 5.2.

CHAPTER 4

SCATTERING PROPERTIES OF TERRAIN IN MICROWAVE BANDS

Calculation of the RCS, σ, of targets or objects is one of the important subjects for target or object detection and identification. RCS is the property of a scattering object, or target, that represent the magnitude of the echo signal returned to the radar by the target. An object exposed to an electromagnetic wave disperses incident energy in all directions. This spatial distribution of energy is called scattering, and the object itself is often called a scatterer. The RCS shows the targets properties as size, shape, nature and orientation where nature of target is related with the roughness, shape, element (permittivity, conductivity etc.) of the target.

As described in Chapter 2, since objects (like islands) over sea may be simulated as artificial scatterers, analyzing their electromagnetic scattering properties is necessary for classification. In this chapter, theoretical background of RCS is discussed first and then, bistatic scattering coefficient of some known objects are compiled from the literature since the scattering properties of natural terrains are represented by scattering coefficient.

In general, RSC is a function of

- Position of transmitter and receiver relative to target,
- Angular orientation of target relative to transmitter and receiver,

- Target geometry and material composition,
- Frequency or wavelength,
- Transmitter and Receiver polarization.

RCS of a target is formulated, in general, as

$$\sigma = 4\pi R^2 \frac{E_r^{\,2}}{E_i^{\,2}} \tag{33}$$

where, R is the range to the target, E_r is the electric field strength of the echo signal back at the radar, and E_i is the electric field strength incident on the target. The derivation of the expression assumes that a target extracts power from an incident wave and then radiates that power uniformly in all directions. Although the vast majority of targets do not scatter energy uniformly in all directions, the definition assumes that they do. This permits one to calculate the scattered power density on the surface of a large sphere of radius *R* centered on the scattering object. *R* is typically taken to be the range from the radar to the target [35].

RCS is therefore a comparison of the scattered power density at the receiver (P_d) with the incident power density at the target (P_r). An equally valid definition of the RCS results when the electric-field strengths in (33) are replaced with the incident and scattered magnetic-field strengths. It is often necessary to measure or calculate the power scattered in some other direction than back to the transmitter, a bistatic situation. A bistatic RCS may be defined for this case as well as for backscattering, provided it is understood that the distance *R* is measured from the target to the receiver. Typical bistatic and monostatic (backscattering) situations are illustrated in Figure 3.

Monostatic (Backscattering):

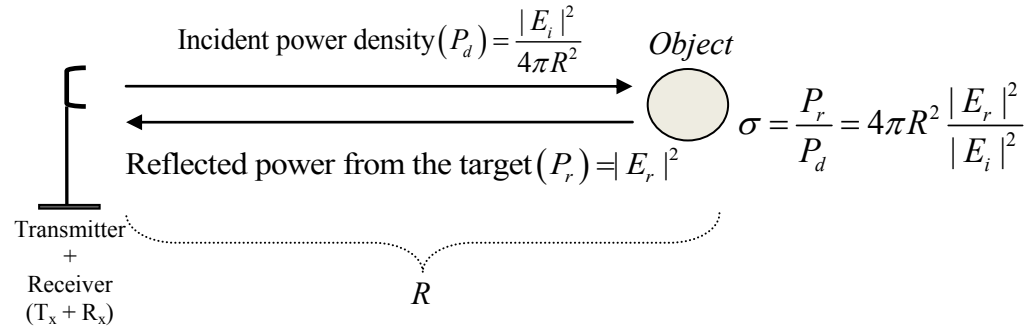

Bistatic:

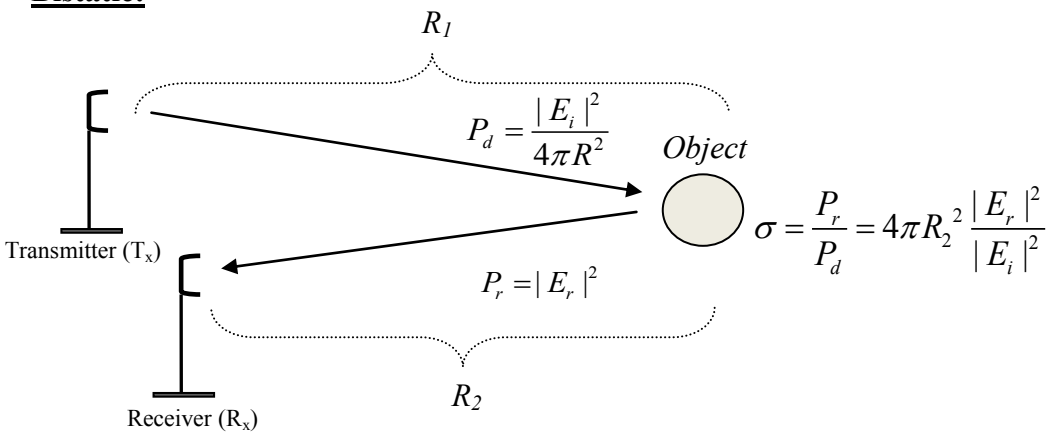

Figure 3 – RCS Geometry for Monostatic and Bistatic System

Since a single number by itself is rarely used to describe a target, there is no standard agreed method for specifying the single-value cross section of a target. A single number is not a complete measure of RCS. There are times, however, when a single number is desired to describe a class of radar target. The average value or the median value might be taken. In this manner, collected bistatic scattering coefficients in the following sections are taken as average value (mean value).

In the following, relationship between scattering coefficient and RCS of a surface clutter is provided.

4.1 Surface Clutter

Radar clutter is defined as unwanted echoes, typically from the ground, sea, rain or other precipitation, chaff, birds, insects, and aurora [36]. However, clutter in here is used positively, i.e., it is used to identify various scatterers over sea for localization. The radar return of transmitter energy scattered by terrain (called surface clutter) from specific area (called the clutter cell area) is a function of the bistatic angle (β). The bistatic angle (β) is the angle subtended at the clutter cell by the lines joining it to the transmitter and receiver that are separated in space. Illustration of β is shown in Figure 4.

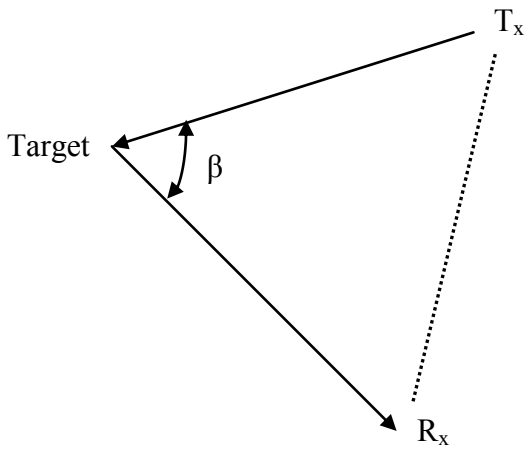

Figure 4 – Illustration of Bistatic Angle

4.2 Clutter Radar Cross Section

The clutter cross-section or bistatic RCS of surface clutter, σ_c, is a measure of the energy scattered from a clutter cell area, A_c, in the direction of the receiver. Again, clutter is used positively to represent a point of an object over sea for localization The bistatic RCS is defined as,

$$\sigma_c = \sigma^0 . A_c \tag{34}$$

where σ^0 is the scattering coefficient, normalized radar cross section (NRCS), or the clutter cross section per unit area of the illuminated surface. The clutter RCS has the dimensions of area and is often expressed in units of [dBm^2] = $10\log_{10}$ [area expressed in square meters]. Therefore, RCS values are expressed relative to 1 m^2 cross-sectional area.

The definition of scattering coefficient, σ^0, is characterizing diffuse scatter (rays reflected in all directions) from rough extended surfaces (surfaces that extend beyond the field of view of the transmitter or receiver) and σ^0 is depending on the type of averaging performed.

Although scattering measurements of terrains in the bistatic radar are proposed in the open literature, only few experimental data sets exist at microwave bands [4-18], and millimeter-wave frequency bands [19-20]. Since these measurements are made by many different investigators, the data is presented using a variety of formats. For example, bistatic scattering coefficients data are plotted in linear, decibel, and normalized units as a function of incidence angle, scattering angle, out-of-plane angle or antenna depression angle. In this study, measurements of scattering coefficients which are given in data plots are obtained by reading line curves (connected points of σ^0) with taking mean values.

Bistatic measurements of σ^0 are reviewed in the following section. Since scatterers are considered in bistatic scattered fields over and around sea, the measurements on land-based objects are considered. According to the GIS, it is informed that islands are covered with forested hills, hilly wooded, rocky surface and agricultural vegetation. Terrain classification is of major importance to classify these scatterers. Therefore, bistatic scattering coefficients of land-based terrains are collected from the open literature. The existing open literature database of σ^0 for terrain is from nineteen principal investigations over the period 1965 to 2006. The most substantial σ^0 data involving incident, θ_i, and scattering angles, θ_s, out-of-plane angles, ϕ, depression angles, ß, antenna polarizations, and frequency bands are given by [4-23] and all are included in Appendix. Measurements data for σ^0 and a discussion is also

provided in the following section. Since [21-22] and [23] are not currently available to read, few references are given in the following section and Appendix.

Coordinate system for bistatic clutter measurements is illustrated in Figure 5.

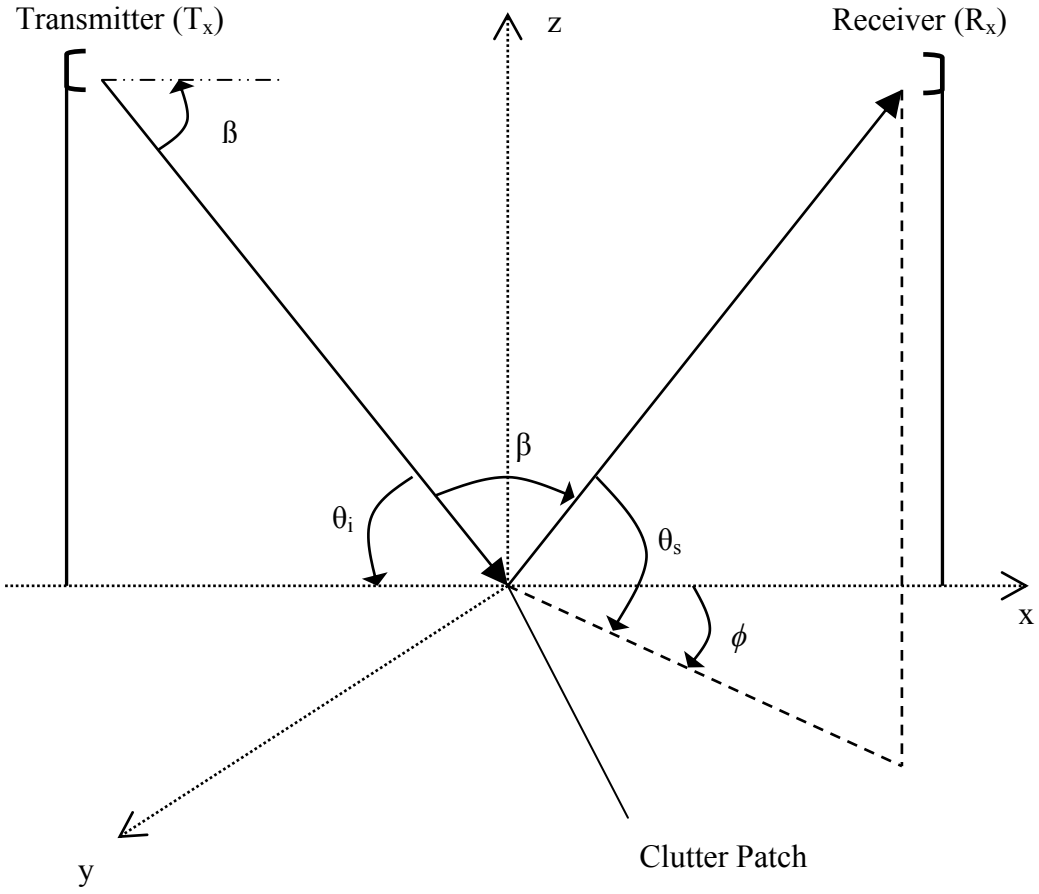

Figure 5 – Geometry of Bistatic Clutter Measurements

where, θ_i is incident angle (in xz plane), θ_s is scattering angle (in plane containing z axis), ϕ is out-of-plane angle (in xy plane) and ß is depression angle.

The incident angle, θ_i, defined with respect to the normal to the surface; the scattering angle, θ_s , is defined from the reflected ray to the surface normal; out-of-plane angle, ϕ, is the horizontal angle of the observer's bearing in surveying; and the depression angle, ß, is defined with respect to the local horizontal at the radar. The incidence angle is the complement of the grazing angle. When the earth's surface is considered smooth and flat, the depression angle and the grazing angle are the same.

When the earth's curvature is taken into account, the depression angle can be quite different from the grazing angle [35].

4.3 Bistatic Scattering Coefficients of Some Known Scatterers

Bistatic radar's transmitting and receiving apertures are separated by a considerable distance. The major variation in a target's bistatic cross section is due to the difference in the respective angles to the target, with range differences playing only a second-order role. There is little data on the bistatic scattering coefficient because the range of geometries is quite large relative to monostatic geometries, and because of experimental difficulties [37].

As discussed in previous section, bistatic scattering coefficients of different scatterers from theoretical and experimental works, which have been published by scientists, are important in the localization problem because bistatic scattering coefficient opens a way for classifying the scatterers in the localization problem. In this context, some bistatic scattering coefficient measurements are collected and analyzed. The problem in considered scenario is based on land-based targets and investigations are made on hilly terrain type of scatterers (such as vegetations, trees, grass, rocky surfaces etc.).

In the open literature, it can be seen that various antenna polarizations are considered for measuring bistatic scattering coefficients of terrains. Antenna polarizations used are shown in Table 1.

Table 1 – Description of Antenna Polarizations

Polarizations	Description
HH	Horizontal to Horizontal polarization is a mode of radar operation in which the transmitting antenna creates an electric field that is oriented in the horizontal plane, and only horizontally polarized component of the scattered energy is picked up by the receiving antenna.
VV	Vertical to Vertical polarization is a mode of radar operation in which the transmitting antenna creates an electric field that is oriented in the vertical plane, and only vertically polarized component of the backscattered energy is picked up by the receiving antenna.
HV	Horizontal transmit - Vertical receive polarization is a mode of radar operation in which the transmitting antenna creates an electric field that is oriented in the horizontal plane, and only vertically polarized component of the backscattered energy is picked up by the receiving antenna.
VH	Vertical transmit - Horizontal receive polarization is a mode of radar operation in which the transmitting antenna creates an electric field that is oriented in the vertical plane, and only horizontally polarized component of the scattered energy is picked up by the receiving antenna.

In this section, microwave frequencies are considered in studying EM scattering properties of objects over and around sea. Experimental data sets of bistatic scattering coefficients of objects are presented at microwave frequency (1-40 GHz bands).

On the other hand, the new system has been worked out to distribute frequencies between the bands. Thus, new system allows faster classification and analysis of a

given emitter. Below is a table of sorts worked out to provide information on the previous and current frequency band designations [38].

Table 2 – Change on Frequency Band Designations

Frequency	Old Band Designation	New Band Designation
500MHz-1GHz	VHF	C
1-2GHz	L	D
2-3GHz	S	E
3-4GHz	S	F
4-6GHz	C	G
6-8GHz	C	H
8-10GHz	X	I
10-20GHz	Ku	J
20-40GHz	Ka	K

To make database of bistatic scattering coefficient measurements for objects over and around sea, we may first meet D.J. McLaughlin who has been working extensively on bistatic scattering coefficient of forests. His group have used same experimental equipments on their researches [4 - 8]. The radar consists of a high-power (1 MW) 2.71GHz transmitter and an incoherent receiver and system separated from each other over a 20 km LOS baseline. The transmitter antenna is on a tower elevated 25 m above the local terrain. The receiver antenna is on a top of a hill of 125m above the local terrain. The measured terrain includes heavily wooded rolling hills covered equal mixture of deciduous and coniferous trees. The antennas view the

terrain surfaces at depression angles below 1°. The clutter cells are measured with different out-of-plane scattering angles from 20° to 70°. In a convention where 0° is the forward scatter direction and 180° is the backscatter direction.

Both VV and HH polarizations have been studied in [4]. Mean bistatic scattering coefficient is -36 dB for VV polarized antennas and -42 dB for HH polarized antennas. VV polarized bistatic scattering coefficient exceeds HH polarized bistatic scattering coefficient by 4-6 dB. Also, scattering coefficients increase by 3 dB after defoliation of the deciduous portion of the tree canopy.

Investigations have been on going to measure bistatic scattering coefficient for cross-polarized transmitter and receiver antennas [5]. The Mean bistatic scattering coefficient of foliated trees is -46 dB for both VH and HV antennas. Measurements shows cross polarized bistatic scattering coefficients are nearly equal.

Another experimental measurement result is [6] that presents multiple polarization measurements with changing the grazing incidence and azimuth scattering angles ranging from 25° to 75° with respect to the forward scatter plane. Mean bistatic scattering coefficients of foliated trees is -39.3 dB for VV, -44.1 dB for HH, -47.3 dB for VH, -47.9 dB for HV. Results show that again forested hills at large bistatic angles and grazing incidence exhibits equal scattering levels for cross-polarized antenna configurations.

After the incoherent (having the same frequency but not the same phase) clutter measurements [4 to 6], a set of coherent (having the same phase or a fixed phase difference), fully - polarimetric bistatic clutter measurements are presented in [7]. Polarimetric scattering measurements of forested hills viewed at grazing incidence and azimuthal scattering angles ranging from 25° to 65° from the forward scatter direction are discussed here. The measurements are obtained from after the defoliation of the tree canopy by using VV, HV, HH and VH polarizations. Mean bistatic scattering coefficient of defoliated trees is -28.3 dB for VV, -38.5 dB for HV, -33.1 dB for HH, -34.7 dB for VH.

New experimental results are conducted over similar terrain at antenna depression angles as high as 2° [8]. The elevations of the transmitter and receiver antennas are 111 m and 200 m in above mean sea level, respectively, and the average terrain height is 70 m above mean sea level. The LOS bistatic baseline separation between the transmitter and receiver antennas was 7.8 km. Azimuthal scattering angles are ranged from 37° to 85° from the forward-scatter direction. The mean bistatic scattering coefficients of defoliated trees is -27.1 dB for vertical transmit and receive (VV). Observed clutter levels are 10-15 dB higher than similar results obtained at lower depression angles.

Conclusions drawn from measurements are in [4-8] as follows:

- The averages of σ^0 for VH and HV polarizations are approximately the same at all measured out-of-plane angles.

- The temporal averages of σ^0 for VV, HH, HV, and VH polarizations have wide variability with changes in spatial position, but they tend to decrease with increases in the out-of-plane angle.

- The averages (temporally then spatially) of σ^0 for VV polarization exceed the averages of σ^0 for HH polarization at all measured out-of-plane angles. The averages (temporally then spatially) of σ^0 for HH polarization decrease more rapidly with increased out-of-plane angle than do the averages of σ^0 for VV polarization.

The important measurement is described by [9] at I-band on the following terrain types: smooth and rough sand, soybean plant foliage, loam with plant stubble and dry grass. The measurements are made in a wide range of incidence and reception angles, azimuth (out-of-plane) angles and antenna polarizations. Numerous curves are provided to illustrate the effects of surface roughness, antenna polarization and angle of incidence. The measurements of the bistatic scattering coefficient of terrain as described here have yielded important results about the scattering from different

types of terrain at various aspect angles and antenna polarizations. Conclusions from the experimental data are follows

- Minimum bistatic scattering coefficient is obtained for most terrains when the out-of-plane angle is 90° ($\phi = 90°$).

- Bistatic scattering coefficient of terrains in the direction of backscatter ($\phi = 180°$) are larger than for $\phi = 90°$.

- For $\phi = 90°$, bistatic scattering coefficient at VV polarization is larger than HH polarization for most terrains.

- Bistatic scattering coefficient in HH polarization is small in specular direction ($\phi = 0°$, $\theta_i = \theta_s$) but comparable to HH or VV scatter for $\phi = 90°$.

The work in [10] provides an overview of I, J, K and M-Band bistatic measurements. The data collection is based on bistatic reflectivity response of sand, gravel, sod and flat plates. The transmitter and receiver are adjusted to have a depression angles of 45°, 40°, 35°, 30°, 25°, 20°, and 15°. The Mean bistatic scattering coefficient of Sand is found as -2.6 dB, -3.6 dB, -2.7 dB, -3.7 dB for VV in M, K, J, I bands respectively. The mean bistatic scattering coefficient of Gravel is -16.1 dB, -12.7 dB, -9.4 dB, -5.5 dB for VV in M, K, J, I bands, respectively. The mean bistatic scattering coefficient of Sod is -17.6 dB, -17.1 dB, -16.9 dB, -15.4 dB for VV in M, K, J, I bands, respectively. Experiments show that the bistatic reflectivity increases as the frequency band decreases. It has been valuable to be able to examine the M, K, J, and I bands in a relatively stable environment and compare the measured responses.

Another study is the bistatic scattering characteristic of forest litter [11]. The effect of forest litter on scattering from the ground is examined throughout the plane of incidence. Measurements are made at I and D bands. The incidence angle θ_i is set to 45° while the receiver angle θ_r is varied over the range from -40° (near backscatter) to +70 in the plane of incidence. The condition of $\theta_i = \theta_r$ corresponds to specular direction. The bistatic scattering response for HH, HV, and VV polarizations are

used for bare sand surface (smooth) and wet pine litter layer. Results of experiments can be concluded as

- For all polarizations bistatic scattering coefficient increases due to the litter at nearly the backscattering angle (θ_i = -40°).

- At nearly the backscattering angle (θ_i = -40°), the presence of the litter also reduces the ratio of σ^0 at co polarized and σ^0 at cross polorized from 8 dB to 5 dB.

- Other different observation is that σ^0 at VV and HH polarization measurements in near backscatter are within 3 dB of each other for all litter types, including the bare sand surface.

Experimental data are obtained by [12] which estimates bistatic scattering coefficient of different terrain types. Measurements are made on two terrain types: dry tall weeds with scrub trees, and dry flat grass at low grazing bistatic angles of 70°, 75°, 80°, and 85°, and 0° to 180° azimuth angle. The measurement system consists of an aircraft transmitter board on; and the receivers are fixed on a tower at the ground. Measurements are made at a wavelength of 3 and 23 cm corresponding to D and I bands, respectively, and for horizontal polarization only. Important results can be concluded as

- Bistatic scattering coefficient larger at I bands than at D band for arbitrary ϕ in non-specular direction.

- Minimum bistatic scattering coefficient is observed when the out-of-plane angle is 90° (ϕ = 90°).

In [13] another experimental data is reported where from estimates of the bistatic scattering coefficient is provided. Measurements are made over snow covered terrain and over an orchard with snow cover. Program results are analyzed and summarized

by another work, [14], that describes the analysis performed on bistatic clutter data collection. This data consists of measurements of bistatic scattering coefficients at two sites, using an airborne transmitter and a tower-mounted receiver. Reflectivity was measured at D and I - bands, at both HH and HV polarizations. The measurement objective is to obtain D and I - bands ground-clutter statistics at large incident angles (θ_i = 60° and 70°) and reflected angles (θ_r = 80°) with out-of-plane (ϕ) angles (between 0° - 180°). This approach intends to use dual-frequency pulsed transmitters in a fly-by aircraft to illuminate the test area at a constant antenna depression angle. The tower-mounted receivers then scan the test area in azimuth at a constant antenna depression angle, measuring the scattering from individual resolution cells at multiple bistatic angles. Measurements are consisting of an apple tree-orchard. The average height of the trees was 25 ft. The ground is completely snow covered. Snow depth is 6 inch and trees' branches are free of snow. Terrain area is the same area of [13]. Experimental result shows that bistatic coefficient of snow covered orchard at cross polarization decreases while increasing out-of-plane angles.

Another bistatic forest scattering model is developed to simulate scattering coefficients from forest canopies in [15]. Two types of canopies are chosen for the bistatic scattering simulation, one is a deciduous tree stand of defoliated aspen. The other is a conifer tree stand of white spruce. Bistatic scattering simulations are fully polarized microwave scattering (HH, VH, VV polarizations) for the canopies in D, G, and I - bands. The frequencies are 1.6, 4.75, and 10 GHz, respectively. Various bistatic observation angle combinations are simulated. For aspen, the angles θ_i = 30°, ϕ = 120° are fixed while θ_s changes from 10° to 70° and for spruce, $\theta_i = \theta_s$ = 45° are fixed while ϕ changes from 0° to 180°. The direction ϕ = 0° is the specular direction, and ϕ = 180° is the backscattering in considered model. Spruce tree densities from 2000 trees/ha to 1000 trees/ha, 666.7 trees/ha, and 500 trees/ha are also given for spruce stand then the model is simulated with observation angles which are described above. In order to adapt this work to our study, 2000 trees/ha density is assigned as dense spruce wooded, and 500 trees/ha is assigned as sparse spruce wooded while collecting the data of bistatic scattering coefficients. It is concluded that bistatic scattering coefficient decreases while density of spruce decreases. It is also indicated

by the authors that bistatic scattering is more sensitive to forest biomass changes than backscattering.

Experiment on the bistatic scattering coefficents of a corn crop and its soil component are given by [16]. Experiments are performed at D - band (1.2 GHz). The bistatic scattering coefficient at HH and HV polarization, as a function of the out-of-plane angle (ϕ) are reported. In considered model, the azimuth scattering angle $\phi = 180°$ corresponds to the backscattering direction, while $\phi = 0°$ corresponds to the specular direction. The data plot simulates the bistatic scattering coefficient of a maize field at medium height (height of 80 cm); the soil moisture content is fixed to 13% and the soil height standard deviation is 1.25 cm. The incidence and scattering angles are set to 25°. Transmitting and receiving antennas are assumed to have a beamwidth of 3°, and are located at a height of 800 km. From the experimental results it is shown that mean of cross polarized bistatic scattering coefficient is 1-2 dB smaller than the mean of co polarized bistatic scattering coefficient for both corn and soil.

In some other investigations in [17, 18], the bistatic radar technique is implemented to improve the classification of vegetations. The bistatic scattering coefficients are calculated at L and C - bands. Moreover, bistatic scattering coefficients in the specular direction is reported as a function of the Plant Water Content (PWC) and data collection are not completed since the function PWC is out of interest in this study.

The bistatic scattering measurements are performed to evaluate the angular variation of the bistatic scattering coefficient of a smooth sand surface, a rough sand surface, and a gravel surface in [19]. The measurements are performed for HH, HV, and VV polarization configurations. Measurement sets are comprised of two indoor major experiments. In the first experiment, incidence and scattering angle fixed at 66° ($\theta_i = \theta_s = 66°$) and out-of-plane angle (ϕ) varied from 10° to 180°. Second experiment is made to extend the results of the first measurements. Bistatic scattering coefficient is measured in fixed incidence angle (θ_i) and scattering angle (θ_s) at 60° as a function of ϕ varied from 10° to 180°. It is noted that in the geometry considered the $\phi = 0°$

corresponds to the backscattering direction, while ϕ = 180° corresponds to the forward direction. As a result, this investigation provides a quantitative reference for the bistatic scattering properties of the type of ground based scatterers. As a result, experiments conclude that

- For smooth sand, HH clutter is larger than VV in specular direction (ϕ = 0°, $\theta_i = \theta_s$) but smaller than VV and HV outside main lobe (at $\phi \approx 180°$).

- Rough sand clutter and gravel clutter are significantly lower in the specular direction (and their main lobes broader) than for smooth sand clutter.

The measurements of the bistatic scattered field from dry rough soil surface is performed at 35 GHz (K-Band) is discussed and the angular dependence of the bistatic scattering coefficients, σ^0, are presented by [20]. The bistatic scattering coefficients of the rough soil surface measured in the forward direction at a fixed incidence angle θ_i = 20° as a function of out-of-plane angle, (ϕ): 0°, 20°, 45°, 80°, 100°, 135°, 160°, and 180°. In the model, forward scattering occurs when ϕ = 0°, while backward scattering occurs when ϕ = 180°. The following conclusions can be drawn:

- HH polarization continues to be stronger than VV polarization in the forward direction and away from the specular point at $\theta_i = \theta_s = 20°$ and ϕ = 0°.

- The depolarization effects are found nearly the same for both VH and HV polarization, it is emphasized that depolarization ratio is insensitive to the scattering angle at all azimuth angles.

The work in [21, 22] provide a general picture over a wide range of conditions. Measurements are performed on forest, rural land and semi desert. Measurements are performed with a transmitter a few meters above the ground, the receiver is located in aircraft with constant antenna depression angles. According to the discussion in [34] about the results of [21,22], measurements first are fit to simple empirical

formulae and then combined with other measurements and theory. A computer algorithm is also described that can calculate clutter spectra for a wide range of conditions using the data provided.

In [23], reflection and tracking data is gathered explicitly to extend the low altitude database. Scattering models are validated against short pulse I - band reflection measurements over beach and sand dunes. Measurements are made with helicopter-borne transmitter and tower-mounted receiver. Conclusions for [23] are drawn as in [34]:

- Specular reflections, when not masked by beach, are larger than diffuse reflections.

- Beach specular reflection is -18.5 dB compared to direct signal power.

As can be seen from the previous discussions, various bistatic scattering coefficients of scatterers are collected, compiled and analyzed from the open literature. After the collection of these bistatic scattering coefficients, the next Chapter is intended to classify the scatterers according to scattering coefficients discussed above for TDOA localization of emitters.

CHAPTER 5

CLASSIFICATION OF SCATTERERS AND EMITTER LOCALIZATION

As discussed in Chapter 2, it is necessary to make a scatterer classification before the choosing scatterers by using GIS as virtual sensors for emitter localization. After given scattering properties of scatterers over sea in Chapter 4, classification table is created in Section 5.1 according to provided bistatic scattering measurements.

The algorithm of closed – form solution of the nonlinear equations for emitter location using TDOA as given in Chapter 3 is also discussed in Section 5.2 and existence of a solution to the quadratic equation in (37) is proposed as it degrades two solution to unique, real and positive solution for emitter localization.

Moreover, this chapter is also intended to test the accuracy of TDOA based emitter localization as stated in Chapter 3. Given approach for emitter localization is implemented to real environment. Simulations and its results are discussed in Section 5.3.

5.1 Classification of Scatterers

As a studied in Chapter 4, in bistatic measurement systems, bistatic scattering coefficient of objects is an important parameter for classifying the scatterers. In this context, experimental bistatic scattering coefficient measurements that are provided from open literature, are discussed in Chapter 4. As stated in Chapter 2,

over sea surface is considered, and it is known that scatterers over sea (like islands) are covered by forested hills, hilly wooded, rocky surface and agricultural vegetation. Hence, only terrain types of islands over sea surface are considered in this section. Therefore, data collection is made such that it includes bistatic scattering coefficients of different terrain types given in Appendix.

As a mentioned in Section 4.2, the most substantial σ^0 data, in terms of incident angle, θ_i, and scattering angles, θ_s, out-of-plane angles, ϕ, depression angles, ß, antenna polarizations, frequency bands and experiment results are given by [4-13] and [15, 16, 19, 20] as summarized in Table 3. Investigations in [14], [17] and [18] are not stated in Table 3 because scattering coefficients of agricultural crops are reported as function of Plant Water Content (PWC) in [17-18]. PWC is not a parameter in our consideration so these references are not stressed in this section. In [14], measurements have been made on snow covered apple tree-orchard. This can not be assumed as an object over and around sea surface. Therefore, it is not discussed in this section, too. Since [21-22] and [23] investigations are not currently available to reach, summary of their measurements are not listed in Table 3 and Table 4.

In Table 3, measurement angles are collected and angle ranges are created including out-of-plane, depression, incidence and reflected angles. On the other hand, antenna polarizations, frequency bands and terrain types corresponding to these angles are all used as a classification parameter.

Table 3– Summary of Measurements for Bistatic Scattering Coefficient, σ^0

Ref.	Surface	Band	Polarization	Measurement Angles				Notes
				θ_i	θ_S	ϕ	ß	
[4-8]	Forested Hills	E	VV, HH, HV, VH	-	-	20-80	≤1	**1)** In all variation of ϕ, mean of σ° for VH and HV are approximately equal and VV exceeds the HH. **2)** Averages of σ° for VV, HH, HV, and VH tend to decrease while increasing ϕ. **3)** 3dB increasing in σ° after defoliation of tree.
[9]	Smooth Sand, Loam, Soybean Foliage / Rough Sand, Loam with stubble,	I	VV, HH, HV	5-30, 10-70	5-30, 5-90	0-145, 0, 180	-	**1)** HH scatter is smaller in specular direction but comparable to HH or VV scatter for ϕ=90° **2)** Minimum scatter at ϕ=90 and scatter larger for VV than HH. **3)** Forward lobe larger for HH than VV **4)** Brewster angle effect is observed for smooth surfaces in specular direction
[10]	Sand, Gravel, Sod	K, J, I	VV	-	-	-	15-45	**1)** Reflectivity increases as the frequency band decreases
[11]	Bare Sand, Sand Surface with	I	VV, HH, HV, VH	-40-70	45	-	-	**1)** The effect of the litter layer is to reduce the specular reflectivity of the ground and to increase scattering in other directions
[12-13]	Scrub Trees with Tall Weeds	D, I	HH, HV	70-80	80	0-105	-	**1)** Scatter larger at 9.4 GHz than at 1.3 GHz for arbitrary ϕ in non-specular direction. **2)** Minimum scatter at ϕ = 90°.
[15]	Aspen, Spruce	D, G, I	HH, VV, VH	30, 45	10-70, 45	120, 0-180	-	**1)** Bistatic scattering coefficient decreases while density of spruce decreases
[16]	Corn, Soil	D	HH, HV	25	25	0-180	-	**1)** Cross polarized bistatic scattering coefficient is 1-2 dB smaller than co polarized for both corn and soil
[19]	Smooth and Rough Sand, Gravel	K	VV, HH, HV, VH	60, 66	60, 66	0-180	-	**1)** For smooth sand, HH is larger than VV in specular direction but smaller than VV and HV outside main lobe. **2)** Rough sand and gravel are lower in the specular direction
[20]	Rough Soil	K	VV, HH, HV, VH	20	0-70	0	-	**1)** HH continues to be stronger than VV in the forward direction and away from the specular point **2)** Mean of σ° found nearly same for both VH and HV

The parameters θ_i, θ_s, ϕ, ß appeared in Table 3 are already described in the Section 4.2.

General reviews and conclusions about the experiments are also summarized in Table 3. Table 4 is intended to get more general statement of bistatic scattering coefficient values. The aim of all these generalizations is to make classification the terrain types easier. It is not possible to specify a single-value scattering coefficient for an object since a single number is not a complete measure of bistatic scattering coefficient. However, a single number can be used to describe a class of object. The average value or the median value might also be taken and in collected bistatic scattering coefficients data from the investigations is taken as average value is taken.

Before creating Table 4, a various assumptions are also made. First of all, antenna polarizations are divided into two sections; cross-polarized (VH/HV) and co-polarized (VV/HH). The bistatic scattering coefficients for co and cross-polarization are averaged over both VV and HH polarizations for co-polarization and both VH and HV for cross-polarization. Averages for σ^0 are, then, calculated as

$$\sigma^0_{av,cross} = \frac{\sigma^0_{VH} + \sigma^0_{HV}}{2} \tag{35}$$

and

$$\sigma^0_{av,co} = \frac{\sigma^0_{VV} + \sigma^0_{HH}}{2} \tag{36}$$

Then, measurement angles (θ_i, θ_s, ϕ, ß) for each terrain types are ignored and scattering coefficient values that are corresponded to these angles are averaged for co and cross polarization for same terrain types at same frequencies.

Beside these, different terrain types are generalized. For example, dry flat grass (smooth), dry flat grass, grassy sod are generalized as grassland, loam with stubble,

soybean foliage and corn are generalized as agricultural, gravel is generalized as rocky surface, foliated tree, defoliated tree, scrub with tall weeds, aspen and spruce are generalized as rural land, loam, sand (smooth), sand (rough), bare sand, sand with pine litter, and soil (rough) are generalized as non-vegetated terrain.

According to frequency bands in Table 4, terrain types can be evaluated as followings:

- For D-Band, according to mean values of for σ^0 grassland, agricultural, rural land and non-vegetated Surface, classification can be made. -18,8 dB, -14,3 dB, -16,7 dB and -19,6 dB corresponds to grassland, agricultural, rural land and non-vegetated surface.
- For E and G-Band, measurements are limited to terrain type of rural land. So that classification for this terrain type can be made in itself and according to mean values of σ^0 for all vegetations can be classified.
- For I-Band, whole terrain types can be classified according to their mean values of σ^0 that are -5,5 dB, -15,3 dB, -16,3 dB, -17 dB and -18,3 dB with respect to rocky surfaces, non-vegetated terrain, grassland, agricultural and rural land.
- For J-Band, grassland, rocky surface and non-vegetated terrain are classified easily due to little information about the scattering coefficients for different terrain clutters. There should be more measurements on σ^0 to a more robust classification, of course.
- For K-Band, grassland, rocky surfaces and non-vegetated terrains are classified easily in L and Ku bands. More σ^0 measurement for only rock surfaces and non-vegetated terrains may be required.

Table 4 – Classification of Scatterers for σ^0 and Frequency Bands

Terrain Type	Polarization	Mean of σ°(dB)						Standard Deviations, SΔ(σ°)					
		Ferquency Band											
		D	E	I	G	J	K	D	E	I	G	J	K
Grassland													
Dry Flat Grass (smooth)	Co	-18,8						0					
Dry Flat Grass	Co				-12,8						2,5		
	Cross				-20,8						3,2		
Grassy Sod	Co				-15,4	-16,9	-17,1				0,6	0	0
Mean		*-19*			*-16*	*-17*	*-17*						
Standard Deviation		*0*			*4,1*								
Agricultural													
Loam with Stubble	Co				-12,3						3,3		
	Cross.				-25,5						6		
Soybean Foliage	Co				-13,6						2,4		
	Cross				-16,5						0,4		
Corn	Co	-13,8						0,4					
	Cross	-14,8						0,4					
Mean		*-14*			*-17*								
Standard Deviation		*0,7*			*5,9*								
Rocky Surfaces													
Gravel	Co				-5,5	-9,4	-12,7				0	0	1,4
	Cross						-8,6						1,5
Mean					*-5,5*	*-9,4*	*-11*						
Standard Deviation					*0*	*0*	*2,9*						
Rural Land													
Foliated Tree	Co		-40,6						2,5				
	Cross		-47						7,1				
	Co		-27,1						7				
Defoliated Tree	Co		-33,9						2,2				
	Cross		-36,6						0,3				
Scrub Trees with Tall Weeds	Co	-9,6			-15,7			5			1,8		
	Cross	-10,2			-18,6			4,6			0,2		
Aspen	Co	-27,1		-20	-21								
	Cross	-28,6		-20,8	-17,9								
Spruce (Dense)	Co	-15,7											
	Cross	-20,4											
Spruce (Sparse)	Co	-5,4											
	Cross	-16,3											
Mean		*-17*	*-37*	*-20*	*-18*								
Standard Deviation		*8,3*	*7,4*	*0,6*	*2,2*								
Non-Vegetated Terrain													
Loam	Co				-15,7						0,3		
	Cross				-23,9						6,1		
Sand (rough)	Co				-9,7		-11,6				4		0,1
	Cross				-23,4		-17,3				5,7		4
Sand (smooth)	Co				-2,6	-2,7	-3,6				9	0	5,7
					-19,6		-10,4				3		0,9
	Cross				-22,4		-17,4				5		4
Bare Sand	Co				-16,3								
	Cross				-25								
Sand with Pine Litter	Co				10								
	Cross				-19,8								
Soil (rough)	Co	-18,4					-7,25	0,8					3,1
	Cross	-20,8					-14,5	0,8					2
Mean		*-20*			*-15*	*-2,7*	*-12*						
Standard Deviation		*1,7*			*11*	*0*	*0*						

Classification process may be understood better, when an EI system is considered. In an EI system, signals are coming from different angles and system separates received signals to clusters by the information of AOA, PW, and RF of the signals. Scatterers are decided from these signal clusters on the basis of scattering coefficients after checking the geography of the region via GIS. Scatterers which have similar parameters but weaker power levels than the others, can be eliminated. Scatterers which have a good ability of scattering coefficient are chosen as a candidate sensor for localization. These candidate sensors are, then, used in localization of the emitter as discussed in the Chapter 2.

5.2 Emitter Localization

The location estimation of an emitter has gained considerable attention and it is one of the important features of an intercept receiver. Using measurement of signals, different methods can be applied to estimate the emitter location. Position estimation from TDOA is one of the commonly used methods. The location is determined using standard complex computation methods that are usually implemented in software.

As discussed before, two dimensional (2D) model is considered in this study. There are three sensors exist. One of the sensors is decided as reference sensor and it is positioned at the origin. Sensors that receive the emitter's signal first then two independent TDOA measurements are performed. Once two measurements are obtained, they are converted into range (distance) differences as described in Chapter 3. Such conversion is simply done by multiplying every TDOA value by the velocity of the signal (speed of light). Therefore, a direct and short derivation of an algorithm based on the closed-form solution of the nonlinear equations for emitter location using TDOA from two sensors is given. As a result, quadratic equation (32) is provided. However, two results ensue, so other information must be used to determine which is correct. In this section, the existence of solution is provided to degrade two real emitter positions to a unique position.

Algorithms solving the location of the emitter using TDOA method are usually software-oriented. In this section, the method proposed in Chapter 3 is implemented in MATLAB.

The algorithms which we proposed are also based on TDOA approaches [2]. The way finding the emitter's location is performed as illustrated in the flowchart of Figure 6.

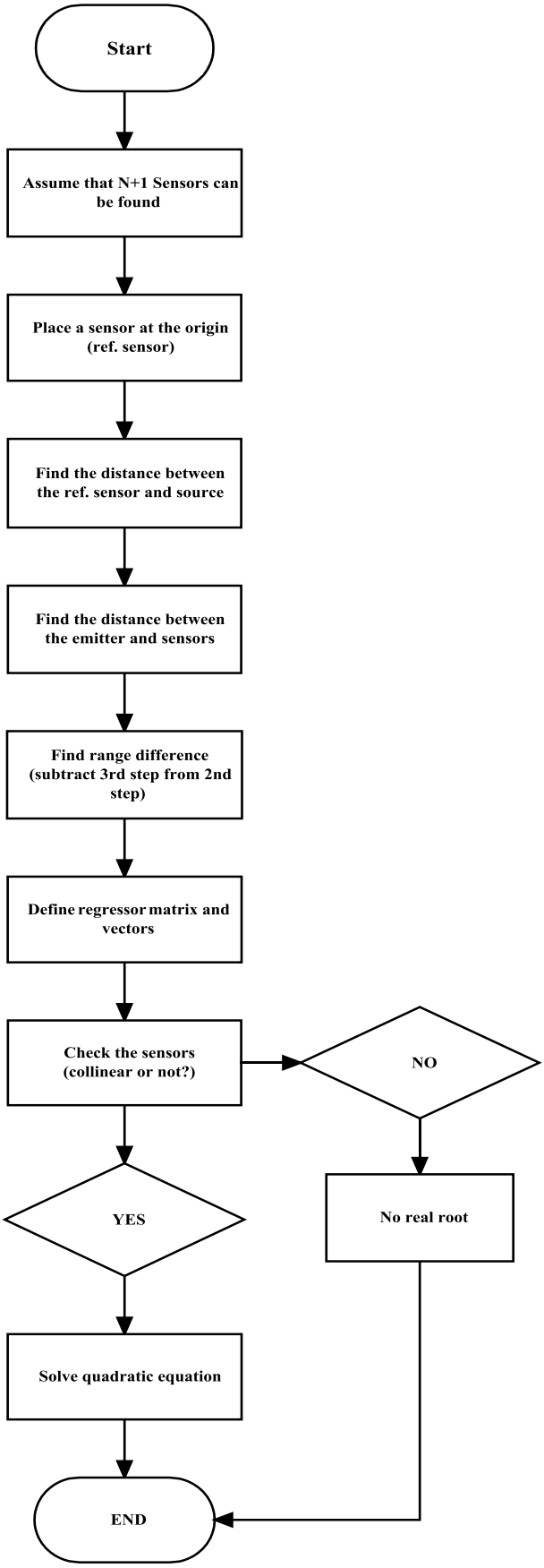

Figure 6 – Flow chart for proposed method

There are some requirements to provide a unique, real, positive solution to the quadratic equation (25). First, the case of two sensors is considered. At least three sensors do not have to be collinear (if slopes of each scatterer positions are the same) as shown in Figure 7. If they are collinear, the regressor matrix $\mathbf{S}_{2x2}$ has not full rank and there remains the possibility that (25) has imaginary roots, where the solution to $\hat{R}_s$. Thus $\hat{\mathbf{E}}$ (22) cannot be found.

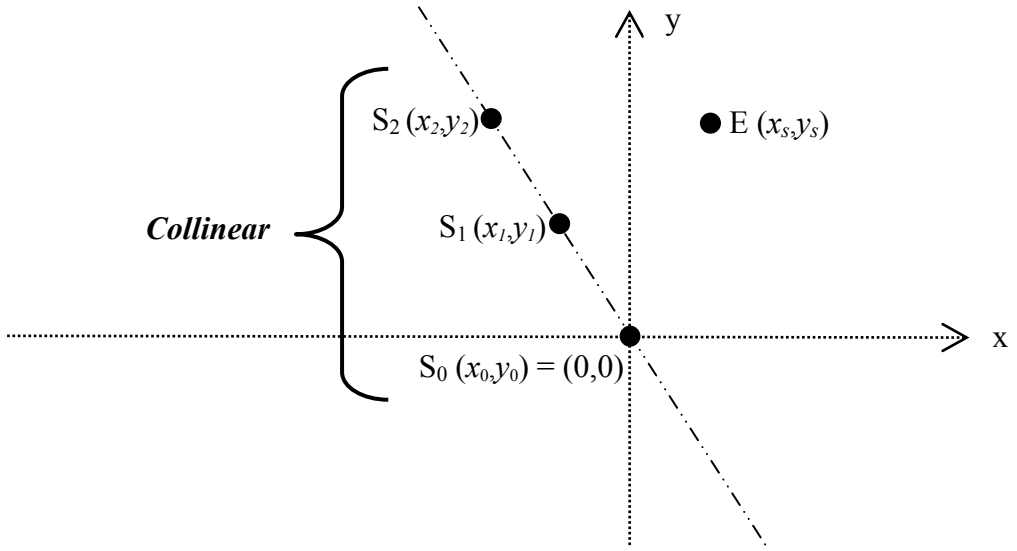

Figure 7 – Collinearity of Sensors

Assumption made above assures that the regressor matrix $\mathbf{S}_{2x2}$ is full rank. The measurement information is contained in the vectors $\mathbf{d}$ (18), $\mathbf{z}$ (17) $\in \Re^2$. After substituting these vectors in to (32), the solutions of the quadratic equation are explicitly given by

$$\hat{R}_s = \frac{\mathbf{d}^T\mathbf{s}(\mathbf{s}^T\mathbf{s})^{-2}\mathbf{s}^T\mathbf{z} \pm \sqrt{[\mathbf{d}^T\mathbf{s}(\mathbf{s}^T\mathbf{s})^{-2}\mathbf{s}^T\mathbf{z}]^2 + \mathbf{z}^T\mathbf{s}(\mathbf{s}^T\mathbf{s})^{-2}\mathbf{s}^T\mathbf{z}\cdot[\mathbf{d}^T\mathbf{s}(\mathbf{s}^T\mathbf{s})^{-2}\mathbf{s}^T\mathbf{d}-1]}}{\mathbf{d}^T\mathbf{s}(\mathbf{s}^T\mathbf{s})^{-2}\mathbf{s}^T\mathbf{d}-1} \quad (37)$$

Assume that assumption made above holds. If

$$\mathbf{d}^T\mathbf{s}(\mathbf{s}^T\mathbf{s})^{-2}\mathbf{s}^T\mathbf{d} < 1 \quad (38)$$

then there exists a unique, real, positive solution to the quadratic equation in (37), and the minus sign applies.

If

$$\mathbf{d}^T\mathbf{s}(\mathbf{s}^T\mathbf{s})^{-2}\mathbf{s}^T\mathbf{d} > 1 \tag{39}$$

and

$$[\mathbf{d}^T\mathbf{s}(\mathbf{s}^T\mathbf{s})^{-2}\mathbf{s}^T\mathbf{z}]^2 \geq \mathbf{z}^T\mathbf{s}(\mathbf{s}^T\mathbf{s})^{-2}\mathbf{s}^T\mathbf{z}\cdot[\mathbf{d}^T\mathbf{s}(\mathbf{s}^T\mathbf{s})^{-2}\mathbf{s}^T\mathbf{d} - 1] \tag{40}$$

then

$$\mathbf{d}^T\mathbf{s}(\mathbf{s}^T\mathbf{s})^{-2}\mathbf{s}^T\mathbf{z} < 1 \tag{41}$$

It implies that there exists a unique, real, positive solution to the quadratic equation in (37) and the plus sign applies.

This method consists simple algebraic equations such as the discriminant of a polynomial. Discriminant of a polynomial is an expression that gives information about the nature of the polynomial's roots. If discriminant is greater than zero, 0 (positive), then there are two distinct real root. It also means a solution exists.

If,

$$\mathbf{d}^T\mathbf{s}(\mathbf{s}^T\mathbf{s})^{-2}\mathbf{s}^T\mathbf{z} > 0 \tag{42}$$

then there exists two real, positive solutions to the quadratic equation (37) because both the plus and the minus signs apply. In this case, it is noted by [2] that at least 4 sensors in 2D are needed to resolve the ambiguity. It should be noted that if

condition (40) does not hold, then a real solution does not exist. Such a case is a modeling error.

5.3 Simulations

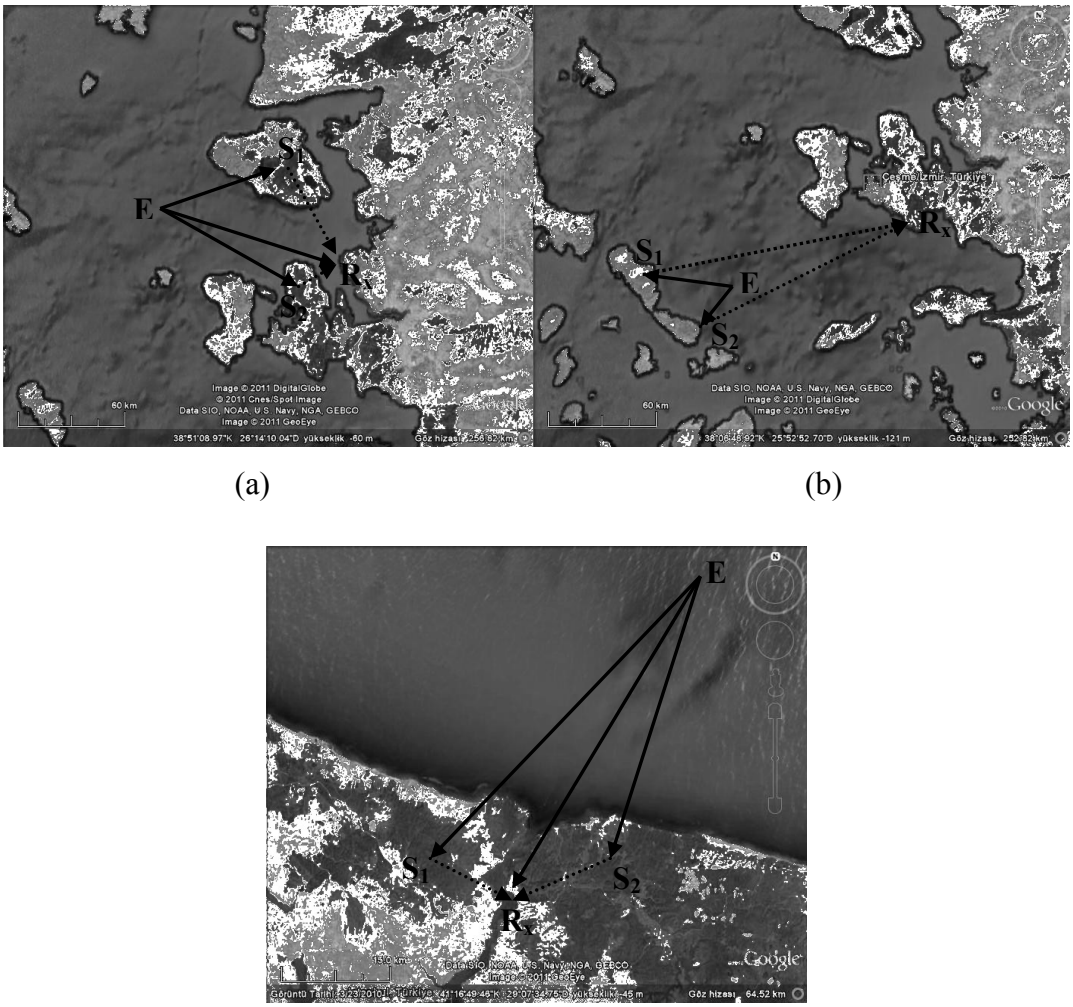

(a) (b)

(c)

Figure 8 – Illustration of Considered Scenarios

In this section, scenario given in Chapter 2 is illustrated. To better illustrate the problem of emitter location estimation using TDOA method, scenarios with three scatterers as shown in Figure 8 (a), (b) and (c) are considered. In the Figure 8, E represents the emitter, S_1 and S_2 represent the scatterers, R_x represents the receiver.

Simulations are conducted to compare the accuracy of the proposed method. In scenario 1, position of one of the scatterer is close to the receiver and other scatterer position is equidistant between the receiver and emitter, positions of scatterers in scenario 2 are close to the emitter but far away from the receiver and in scenario 3, scatterers are so close to the emitter. Scenario 3 is also considered differently from other scenarios due to its geographic location. Scatterers are positioned at the top of hills in Marmara Region (around Istanbul) in Turkey and position of emitter is assumed in Black Sea.

In scenario 1 and 2, the emitter is located at $\mathrm{E}(x_S, y_S)$ over Aegean Sea. As discussed in Chapter 3, in TDOA based emitter localization a reference sensor is positioned at the origin. In this context, the receiver as the reference sensor is positioned at coordinates $S_0(0,0)$ on Aegean Region in Turkey. From the discussion in Chapter 2, two islands that are artificial scatterers in Aegean Sea are chosen as the candidate sensors for emitter localization. These islands are covered with scrub trees, rocky surface, grass, sand and forests. Bistatic scattering coefficients, σ^0, of these terrain types are stated in Appendix in detail, and classification of these terrain types is provided in Table 4. Although positions of the islands are known, to think a little more realistic, new calculations are necessary for determining islands' position in 2D. From the geometry, if one point and the slope are known in 2D Cartesian coordinate system, then the line is set. In this context, ranges between the islands and the receiver are obtained by using a satellite map. Slope is calculated from tangent value of angle between an island to receiver and known point is a receiver position that is positioned at $S_0(0,0)$. Point-slope equation of a line is therefore used to define new position of islands.

5.3.1 Analysis; Scenario 1

To apply proposed method to real scenario, scatterer positions are determined by using point-slope equation of a line. Scatterer positions are determined at new positions which are $S_1(49827, 33425), S_2(-14088, 26486)$ for scenario 1 in Figure 9.

In scenario 1, according to GIS, islands as the scatterers are covered with vegetation of scrub trees with tall weeds, foliated tree and hills. These terrain types can be classified as rural land and rocky surface as stated in Table 4. Hills on islands are important scatterers because of their shapes. These types of hills on lands in Aegean Sea are look like walls, so that hilly terrains might be candidate scatterers.

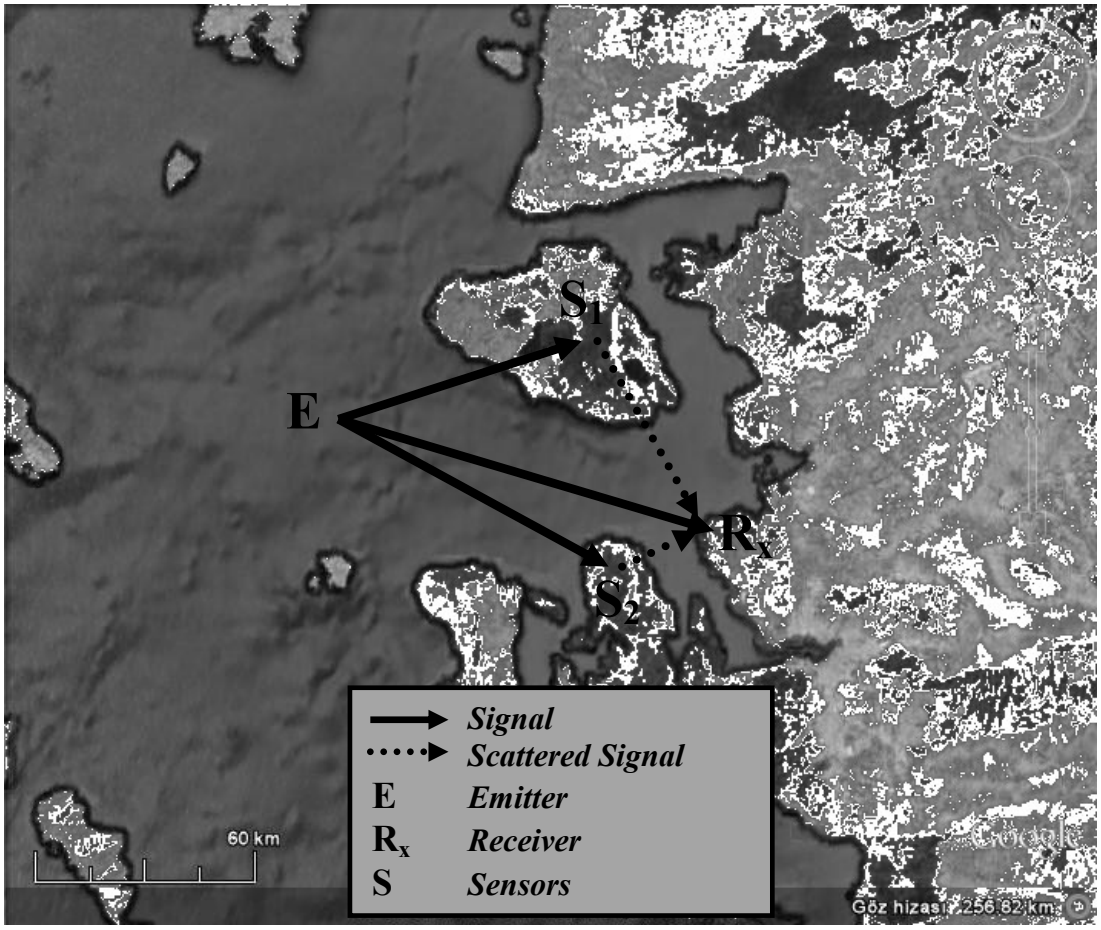

Figure 9 – Scenario Illustration 1

To implement proposed method, first assign position of the receiver (S_0) and scatterers (S_1, S_2) from Figure 9 as

$$S_0 = [0 \quad 0]^T \text{ m}, \quad S_1 = [49827 \quad 33425]^T \text{ m}, \quad S_2 = [-14088 \quad 26486]^T \text{ m}.$$

Moreover, the emitter position is assumed to be $E = [35883 \quad 98678]^T$ m,

after applying proposed approach to measure the emitter location, the emitter position is determined by the TDOA algorithm as

$$xs1 = \begin{bmatrix} 35883.00000000006 & 98678.00000000112 \end{bmatrix}^T \text{ m.}$$

For a realistic scenario, the time arrival error may be introduced into the model since the shape of hills on islands look like "wall" and then signals may reflect different points. From the (2), it is dedicated that TDOAs are directly proportional to the difference in distance between the emitter and the scatterers, simply the RDs. Based on these facts, it is evident that time of arrival error causes range error. In this case, 20% of time of arrival measurement error is assumed for realistic scenario. New measurements are performed time of arrival error. With 20% time of arrival error, 1000 snapshot are generated for each scenario. Emitter position and mean value of candidate emitter positions are shown in Figure 10 for 1000 runs. Scatterer positions and assumed emitter position are also shown in Figure 10.

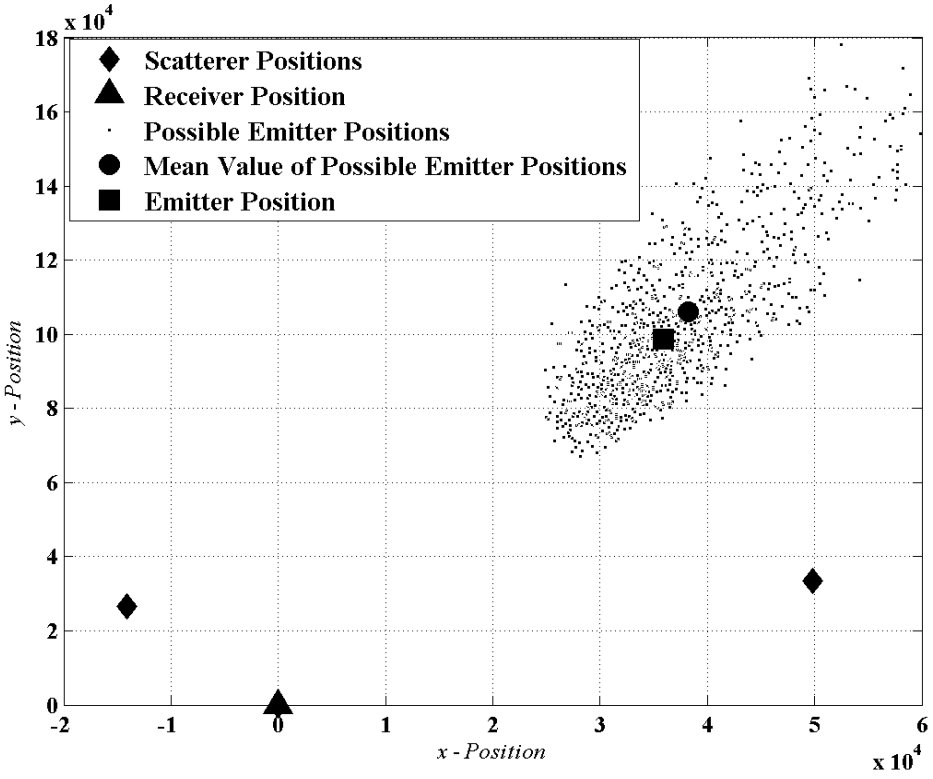

Figure 10 – Illustration of Emitter, Receiver and Sensor Positions with 20% Error in Time of Arrivals (Scenario 1)

Mean value of candidate emitter positions (ΔE) is obtained as

$$\Delta E = \begin{bmatrix} 38210 & 105960 \end{bmatrix}^T \text{m},$$

1000 candidate emitter positions (ΔE) are compared with the emitter position (x_S, y_S). Then measurement errors are calculated. Mean value of measurement error $(\Delta \varepsilon)$ for emitter position is given by

$$\Delta \varepsilon = \begin{bmatrix} 2323.5 & 7280.1 \end{bmatrix}^T \text{m}.$$

It indicates that emitter location can be estimated with an average error of 7.3% if an error of 20% in time of arrival measurement is introduced. This corresponds to a location error of $\begin{bmatrix} 2323.5 & 7280.1 \end{bmatrix}^T$ m when the transmitter location is positioned at $\begin{bmatrix} 35883 & 98678 \end{bmatrix}^T$ m. It can be seen that emitter position is estimated with an error range of approximately 8 km if the time measurement error is introduced to the proposed method. Table 5 shows different artificial time measurement errors to estimation of emitter location.

Table 5 – Emitter Location Estimations with Time Measurement Errors for Scenario 1

True Emitter Location = [35883 98678]^T		
Time Measurement Error (%)	**Measured Location of Emitter (m)**	**Average Error**
5%	[35952 98926]^T	0.25%
10%	[36160 99556]^T	0.88%
15%	[36860 102000]^T	3.3%
20%	[38210 105960]^T	7.3%

5.3.2Analysis; Scenario 2

Other scenario illustration is also considered in Aegean Sea as shown in Figure 11. Again, signals are scattered from the islands and according to GIS, these islands are covered with a terrain of scrub trees with tall weeds and hills. Their scattering coefficients can be analyzed in Table 4. Hereby, these terrain types are classified as Rural Land and Rocky Surface such as terrain types of islands in scenario 1. Also hills have similar shapes of scenario 1.

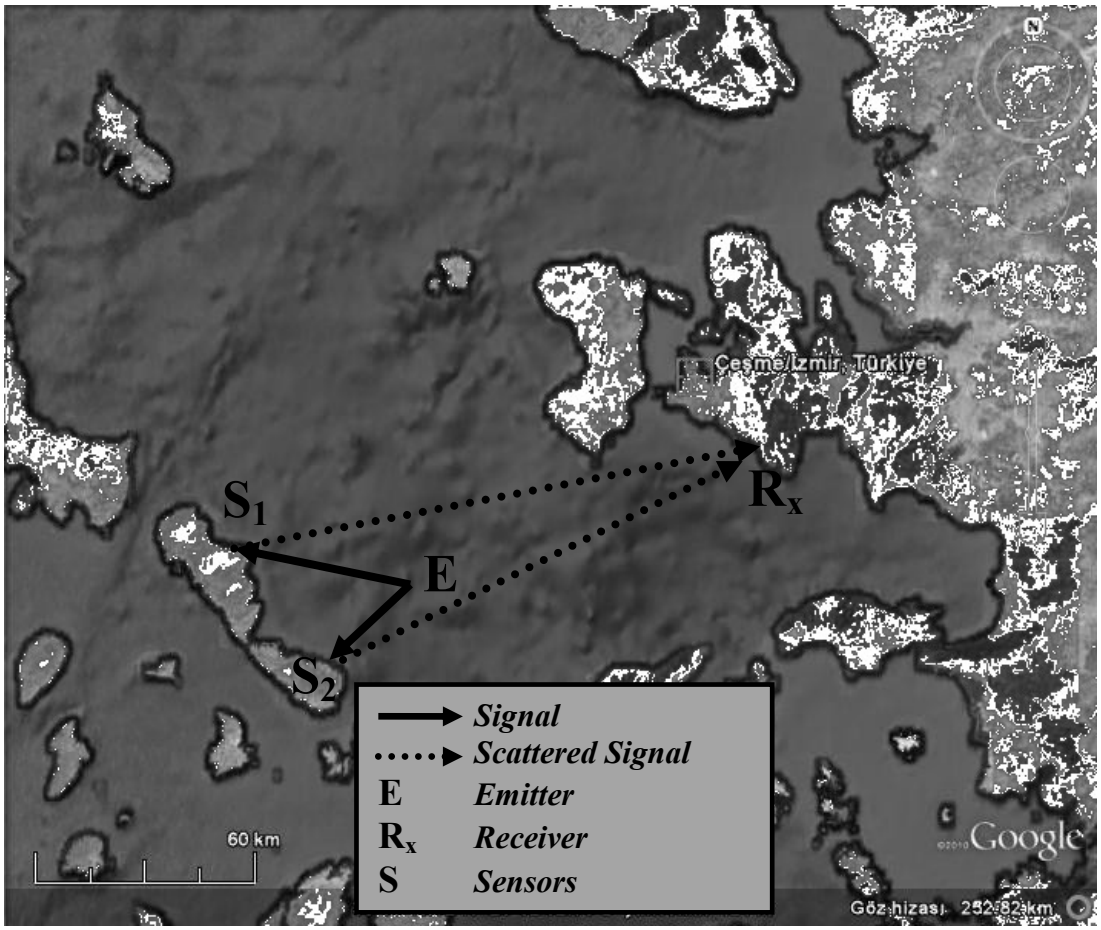

Figure 1 – Scenario Illustration 2

However, this model is a little bit different from the one in Figure 9. In this model, signals are travelling through the islands (scatterers), then scattered signals are received by the receiver in opposite direction since emitter position (x_S, y_S) is considered in between an island in Aegean Sea and head-island in Aegean region.

To find position of the scatterers in Figure 11, new positions are assigned at $S_1(-12010, 20778)$, $S_2(-29546, 5200)$ after using same calculations in scenario 1.

Then, position of the receiver (S_0) and scatterers (S_1, S_2) are defined by using point - slope equation of a line as

$$S_0 = [0 \quad 0]^T \text{ m}, \; S_1 = [-30147.2 \quad 141691.8]^T \text{ m}, \; S_2 = [-60899 \quad 119362]^T \text{ m},$$

and the emitter position is assumed at $E = [-34202 \quad 94055.5]^T$ m.

After using process of proposed localization approach, emitter location can be estimated as

$$xs1 = [-34202.00000000008 \quad 94055.50000000005]^T \text{ m}.$$

Observations on implementation of proposed method by introducing time of arrival measurement error to the system are shown in Figure 12.

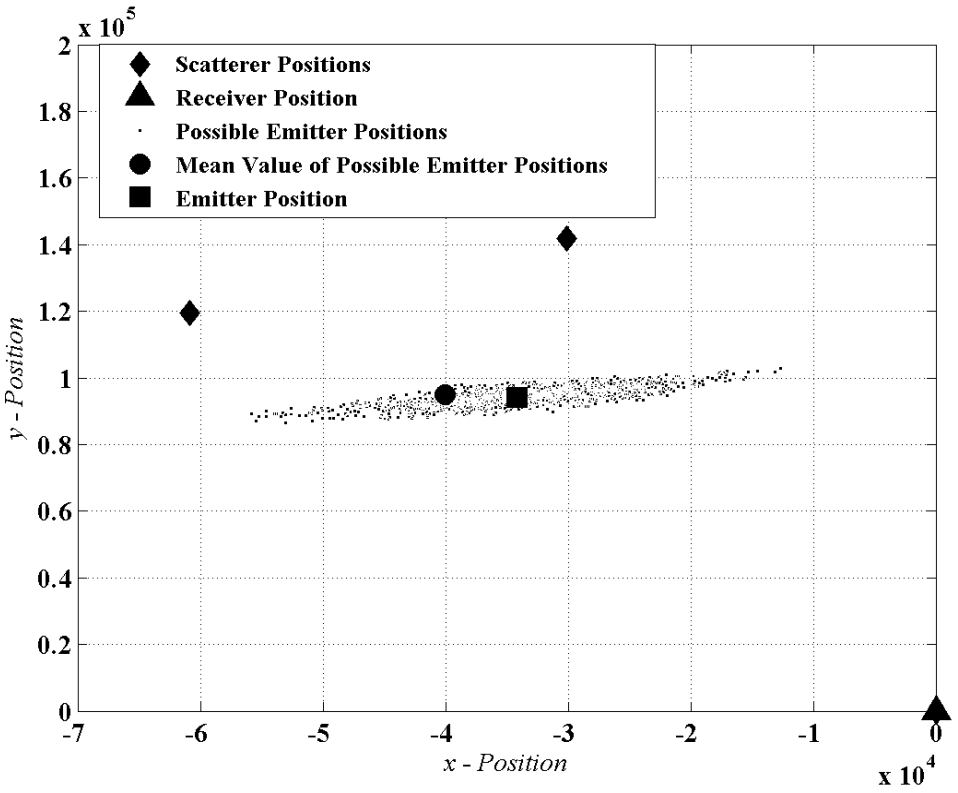

Figure 2 – Illustration of Emitter, Receiver and Sensor Positions with 20% Error in Time of Arrivals (Scenario 2)

In the scenario 2, mean value of candidate emitter positions (ΔE) is calculated as,

$$\Delta E = \left[-40019 \quad 94877\right]^T \text{m},$$

and the mean value of measurement error $(\Delta \varepsilon)$ for emitter position given as,

$$\Delta \varepsilon = \left[\text{-}5817.2 \quad 821.9\right]^T \text{m}.$$

It shows that if the time measurement error is introduced to the proposed method, emitter position will be estimated with in an error range of approximately 6 km.

Measured error for emitter location in scenario 2 is calculated as 5.87%. This means, time measurement error of 20% causes emitter location estimation within an error of 5.87%. This corresponds to a location error of $\left[\text{-}5817.2 \quad 821.9\right]^T$ m when the transmitter location is positioned at $\left[-34202 \quad 94055.5\right]^T$ m.

Simulation results of determining emitter location at different time measurements are shown in Table 6.

Table 6 - Emitter Location Estimations with Time Measurement Errors for Scenario 2

True Emitter Location = [-34202 94055.5]^T		
Time Measurement Error (%)	**Measured Location of Emitter (m)**	**Average Error**
5%	[-34142 94078]^T	0.06%
10%	[-34321 94028]^T	0.12%
15%	[-34506 94089]^T	0.3%
20%	[-40019 94877]^T	5.87%

5.3.3Analysis; Scenario 3

Another scenario as can be seen in Figure 13 is considered to implement given approach for emitter localization around sea.

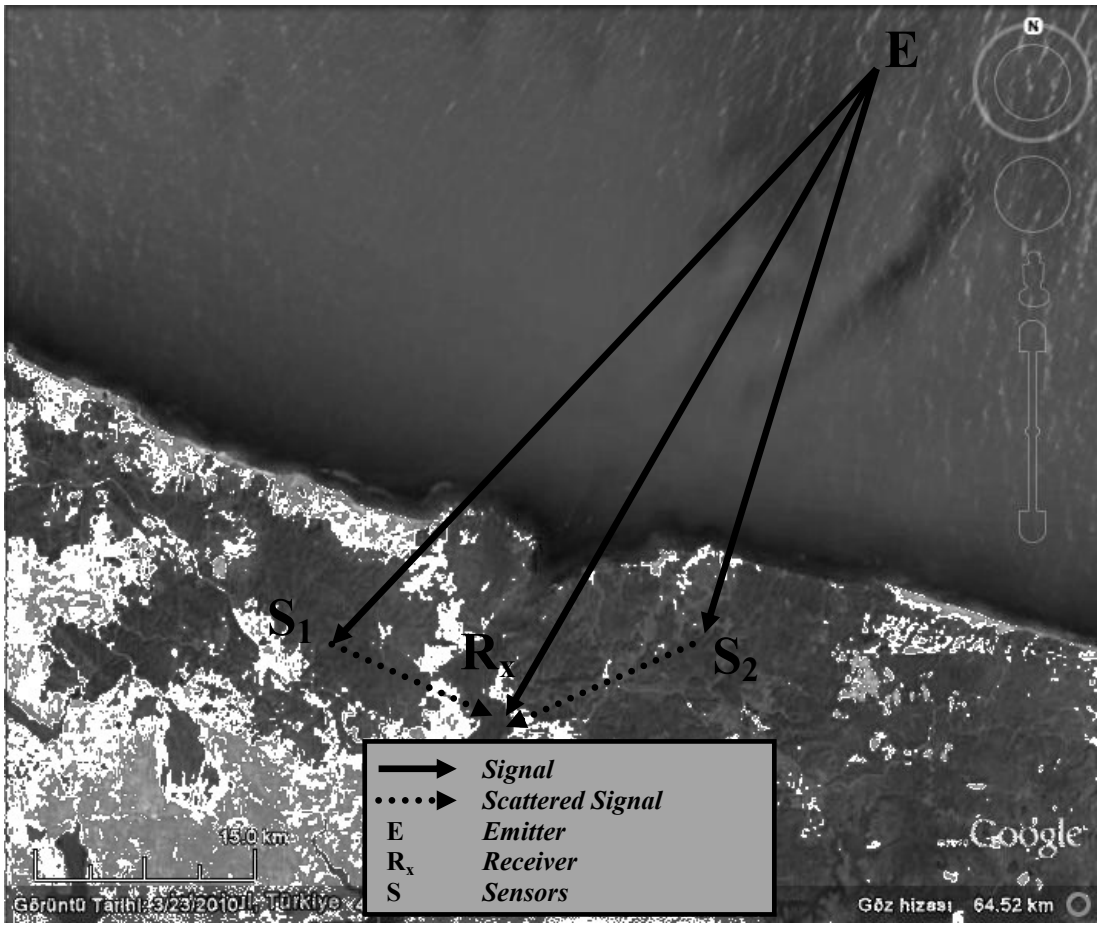

Figure 3 – Scenario Illustration 3

Scenario 3, as shown in Figure 13, is considered in Black Sea. In this scenario there is no islands considered. Signals travelled from the Emitter in Black Sea, are scattered from the hilly terrains of Bosphorus, around the Istanbul. From the GIS, it is observed that scatterers are covered with rocks and foliated trees. These terrain types might be classified as rural land and rocky surface, which are stated in Table 4.

Assign position of the receiver (S_0) and scatterers (S_1, S_2) to find new positions by using point- slope equation of a line

$$S_0 = [0 \quad 0]^T \text{ m}, \; S_1 = [24195.6 \quad 6290.8]^T \text{ m}, \; S_2 = [27189.2 \quad 12778.9]^T \text{ m},$$

the emitter position is assumed at $E = [42261.8 \quad 90630.7]^T$ m.

Then the emitter position is estimated by proposed localization method as

$$xs1 = \begin{bmatrix} 44374.90000000000 & 95406.09999999998 \end{bmatrix}^T \text{ m.}$$

Using same procedure to obtain estimated emitter position when the time of arrival error is introduced to the system, candidate emitter positions are given in Figure 14. Receiver location, position of the scatterers and mean value of candidate emitter positions are also shown in Figure 14.

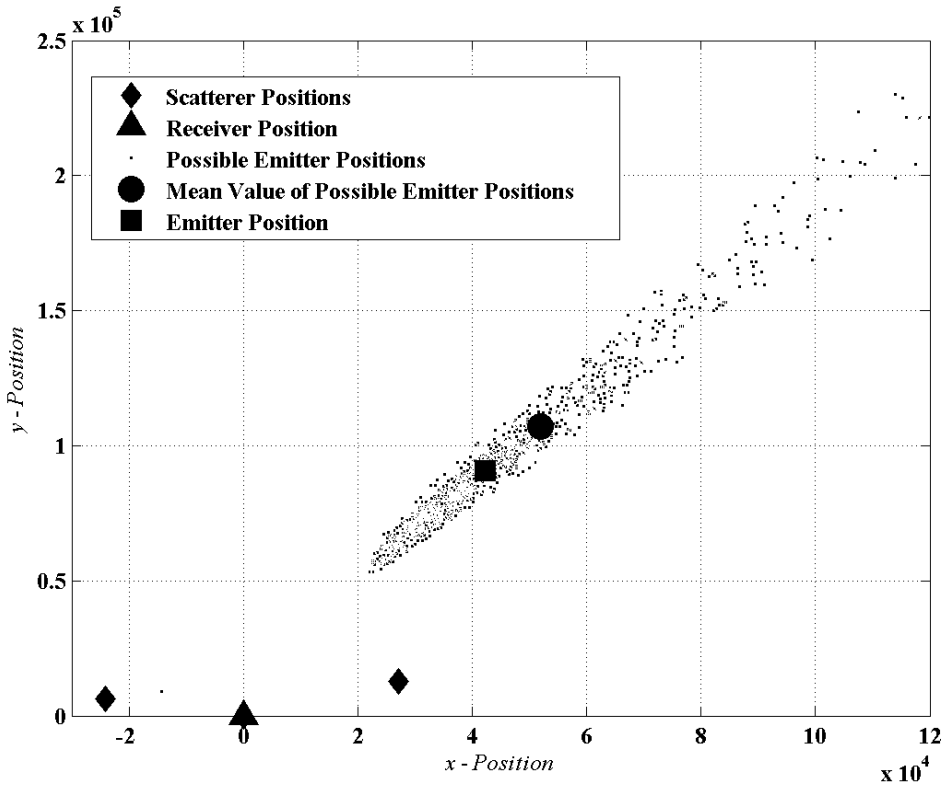

Figure 4 – Illustration of Emitter, Receive and Sensor Positions with 20% Error in Time of Arrivals (Scenario 3)

Mean value of candidate emitter positions (ΔE) are calculated as

$$\Delta E = \begin{bmatrix} 51930 & 107240 \end{bmatrix}^T \text{ m,}$$

and the mean value of measurement error $(\Delta\varepsilon)$ for emitter position is given as

$$\Delta\varepsilon = \begin{bmatrix} 9668.2 & 82441 \end{bmatrix}^T \text{m}.$$

In this scenario, time measurement error of 20% causes 18.3% of error in determining the emitter location. It corresponds to a location error of $\begin{bmatrix} 9668.2 & 82441 \end{bmatrix}^T$ m when the emitter location is positioned as $\begin{bmatrix} 42261.8 & 90630.7 \end{bmatrix}^T$ m.

Thus, emitter position can be estimated with an error range of approximately 19 km if the measurement error is introduced to the system by using the proposed method. This error rate is higher than the other scenarios. According to this result, it can be concluded that location measurement error increases when the positions of scatterers are so close to the receiver.

Another simulation results on different time measurement errors to determine emitter location are shown in Table 7.

Table 7 - Emitter Location Estimations with Time Measurement Errors for Scenario 3

True Emitter Location = [42261.8 90630.7]^T		
Time Measurement Error (%)	**Measured Location of Emitter (m)**	**Average Error**
5%	$[42667 \quad 91431]^T$	0.9%
10%	$[44522 \quad 94529]^T$	4.3%
15%	$[46788 \quad 98466]^T$	8.6%
20%	$[51930 \quad 107240]^T$	18.3%

As a result, accuracy of TDOA based emitter localization from two scatterers is tested in 2D. Stated methods and specific cases in Chapter 3 and Section 5.2 are implemented to real scenarios. As can be seen in this section, from the simulation results there exists a unique, real, and positive solution for emitter localization. Time of arrival error is also introduced. New measurements are performed with time of arrival errors. According to introduced time of arrival error, emitter position is estimated with an error range. Location of the emitter is also measured in order to introduced different time measurement errors.

CHAPTER 6

CONCLUSIONS

Geolocation techniques for EI systems and EM scattering properties of objects over and around the sea are studied. Developments of methods to use scattered signals for location finding systems and scattering of EM waves from scatterers such as islands over the sea in microwave bands are analyzed. It is observed that classification can be made for land-based terrains at microwave bands although there are few measurements on bistatic scattering properties of land-based terrains. That classification provides the required information for designing of future bistatic radar system for remote sensing and military applications such as emitter localization.

First, discussion on TDOA based emitter localization is given. The structure of emitter localization approach is based on

i. An algorithm that is basis on closed - form solution of the nonlinear equations for emitter localization using TDOA measurements from two sensors,
ii. Existence of a solution is provided to get positive, unique and exact emitter location to nonlinear equation (part i) as two results are ensued.

TDOA based emitter localization is advantageous among other localization techniques. These methods require antenna calibration, which is not necessary with TDOA. In addition, TDOA measured by using arrival times of signals received by multiple passive sensors. Therefore, no knowledge about the waveform of the received signal is required as its other important advantage. Provided

localization approach is implemented in real environment to test its accuracy. Two islands over the Aegean Sea are considered as the artificial scatterers. These scatterers are assumed as virtual sensors. From the simulation results, it is shown that, there exists a unique, real, and positive solution for emitter localization. TDOAs are directly proportional to the difference in distance between the emitter and the scatterers as dedicated in (5). This is called range differences (RDs) also. Thus, it can be said that time of arrival error causes range error in general. To sum up, different measurement errors are introduced to the system as can be seen in Chapter 5. Location of emitter is estimated by using these measurement errors and according to simulation results an average error for measured location of emitter is analyzed. An error range is also defined for measured emitter location. According to simulation results, emitter position is estimated with an error range of 8 km for scenario 1, 6 km for scenario 2, and 19 km for scenario 3, if the 20% of time measurement error is introduced into the model. It is also provided that the location measurement error increases when the positions of scatterers are so close to the receiver. Therefore, it is concluded that the accuracy of localization method is insufficient when the positions of scatterers are so close to the receiver. In an EI system, positions of scatterers are close to the receiver such as scenario 3. According to this situation, new positions of scatterers are assigned as close to receiver for testing the accuracy of proposed localization method. According to simulation results, it is observed that the system as used proposed localization method may tolerate the time measurement error up to 3%.

Next, bistatic scattering measurements of some known scatterers over and around the sea is presented. First, an extended research is made on open literature and bistatic scattering coefficients of different objects are collected since bistatic scattering coefficient is an important parameter for classifying objects. From the collected scattering coefficients, a data table is made as can be seen in Appendix. According to collected data of generalized mean bistatic scattering coefficient of different terrain types, Table 3 is created. This table is a summary of bistatic scattering coefficient measurements of the literature. After that, Table 4 is created to classify the terrain types, which are vegetations of scatterers over and around sea in considered scenarios.

As a future work,

- Accuracy of localization method is insufficient when the positions of scatterers are so close to the receiver in case of introducing time of arrival error into the model. Thus, accuracy of proposed method for emitter localization may be improved.

- Ships and bays are the targets that a radar can face over and around sea and there are numerous studies in literature about this subject. Thus, these can be realized as scatterers and it can be inserted to our considerations. Hence, bistatic scattering properties of ships and bays should be investigated to enriched object classification.

- Multipath propagation effects for intercept receivers in naval applications should be studied and bistatic ocean or sea surface scattering properties should be analyzed.

REFERENCES

[1] R. A.Poisel, "Introduction to Communication Electronic Warfare Systems", Narwood, MA: Artech House, 2002, Chapter 12, pp.403-409.

[2] G. Mellen, M. Pachter, J. Raquet , "Closed-Form Solution For Determining Emitter Location Using Time Difference Of Arrival Measurements", IEEE Transactions on Aerospace and Electronic Systems, Vol. 39, No. 3, pp. 1056-1058, July 2003.

[3] Knott, F. Eugene, J. F. Shaeffer, and M. T. Tuley, "Radar Cross Section", Raleigh, SciTech, 2004 Chapter 3, pp.64-71.

[4] D.J. McLaughlin, E. Boltniew, Y. Wu and R.S. Raghavan, "Low Grazing Angle Bistatic NRCS of Forested Clutter", Electronics Letters Online No: 19941024, IEE. Vol. 30, No. 18, September 1994, pp.1532-1533.

[5] D.J. McLaughlin, E. Boltniew, R.S. Raghavan and M.J. Sowa, "Crosspolarised Bistatic Clutter Measurements", Electronics Letters Online No: 19950323, IEE. Vol. 31, No. 6, December 1995, pp.490-491.

[6] D.J. McLaughlin, R.S. Raghavan, W.G. Stevens and M.J. Sowa, "Bistatic Terrain Clutter Dependence on Out-of-Plane Scattering Angle", Electronics Letters Online No: 19950867, IEE. Vol. 31, No. 15, May 1995, pp.1291-1292.

[7] D.J. McLaughlin and M.J. Sowa, "Experiments in Bistatic Scattering Phenomenology", Radar Conference, 1997, IEEE National, May 1997, pp.154-159.

[8] D.J. McLaughlin, W.G. Stevens, M.J. Sowa, B. Weijers and X. Zhang, "Bistatic Scattering Behaviour of Forested Hills at Grazing Incidence", Electronics Letters Online No: 20010511, IEE. Vol. 37, No. 12, May 1995, pp.783-784.

[9] S.T Cost, "Measurements of the Bistatic Echo Area of Terrain at X-Band", Ohio State University, 1965.

[10] B. L. Matkin, J. H. Mullins, T. J. Ferster and P. J. Vanderford, “Bistatic Reflectivity Measurements on Various Terrains at X, Ku, Ka and W-Band Frequencies”, Radar Conference, IEEE, August 2002, pp.266-271.

[11] DeRoo, Y. Kuga, M. C. Dobson, and F. T. Ulaby, “Bistatic Radar Scattering From Organic Debris of a Forest Floor”, Geoscience and Remote Sensing Symposium, 1991. IGARSS '91. Remote Sensing: Global Monitoring for Earth Management. Vol. I, 3-6 Jun 1991, pp. 10.

[12] R.W. Larson, A.L. Maffett, R.C. Heimiller, A.F. Fromm, E.L. Johansen, R.F. Rawson and F.L. Smith, “Bistatic Clutter Measurements”, IEEE Transactions on Antennas and Propagation, Vol. Ap-26, No.6, November 1978, pp.801-804.

[13] R.W Larson, “Bistatic Clutter Data Measurements Data Program”, RADC-TR-77-389 Final Technical Report, November 1977.

[14] R.E. Vander Schuur, P.G. Tomlinson, “Bistatic Clutter Analysis”, Descision-Science Applications, Inc., Final Technical Report DSA-106, April 1979, AD-A069385.

[15] P. Liang, L.E. Pierce, and M. Moghaddam, “Radiative Transfer Model for Microwave Bistatic Scattering from Forest Canopies”, Geoscience and Remote Sensing, IEEE, Vol. 43, Issue: 11, Nov. 2005 pp. 2470.

[16] A.D. Vecchia, P. Ferrazzoli, L. Guerriero, I. Cacucci, M. Marzano, N. Pierdicca, F. Ticconi, “Optimization of Bistatic Radar Configurations for Vegetation Monitoring”, Geoscience and Remote Sensing Symposium, 2006. IGARSS 2006. IEEE, July 31 - Aug. 4 2006, pp. 1220.

[17] P. Ferrazzoli, L. Guerriero, D. Solimini, “Comparison between Predicted Performances of Bistatic and Monostatic Radar in Vegetation Monitoring”, Geoscience and Remote Sensing Symposium, 1994. IGARSS '94, IEEE, Vol. 3, 8-12 Aug 1994, pp. 1850 – 1852.

[18] P. Ferrazzoli, L. Guerriero, D. Solimini, “Simulating Bistatic Scatter From Surfaces Covered with Vegetation”, Journal of Electromagnetic Waves and Applications, Vol. 14, Number 2, 2000 , pp. 233-248(16).

[19] F.T. Ulaby, T.E. Van Deventer, J.R. East, T.F. Haddock, M.E. Coluzzi, “Millimeter-wave bistatic scattering from ground and vegetation targets”, IEEE Geoscience and Remote Sensing, V. 26, No. 3, May 1988.

[20] A. Y. Nashashibi, and F. T. Ulaby, “Millimeter-Wave Polarimetric Bistatic Radar Scattering from Rough Soil Surfaces”, Geoscience and Remote Sensing, IEEE, Vol. 2, 2003, pp. 788.

[21] A.R. Domville, “The Bistatic Reflection from Land and Sea of X-Band Radio Waves, Part I, “GEC (Electronics) Ltd., Stanmore, England, Memorandum SLM1802, July 1967.

[22] A.R. Domville, “The Bistatic Reflection from Land and Sea of X-Band Radio Waves, Part II-supplement, “GEC (Electronics) Ltd., Stanmore, England, Memorandum SLM2116, July 1969.

[23] P.E. Cornwell and J. Lancaster, “Low-altitude Tracking Over Rough Surfaces II: Experimental and Model Comparisons”, in IEEE EASCON-79 Record, Oct. 1979, pp.235-248.

[24] N. J. Willis, “Bistatic Radar”, Raleigh, SciTech Publishing, 2005, Chapter 1, pp. 1.

[25] D. J. Torrieri, “Statistical Theory of Passive Location Systems”, IEEE Transactions on Aerospace and Electronic Systems, Vol. AES-20, No. 2, March 1984.

[26] S. Camlica, “Recursive Passive Localization Methods Using Time Difference of Arrival”, Master Thesis, METU, Sept. 2009.

[27] A. Dersan and Y. Tanık, “Passive Radar Localization by Time Difference of Arrival”, IEEE MILCOM Proceedings, vol.2, pp.1251-1257, Feb. 2002.

[28] R. Schmidt, “Least Squares Range Difference Location”, IEEE Transactions on Aerospace and Electronic Systems, Vol. 32, pp.234-242, Jan. 1996.

[29] R. Schmidt, “A new approach to geometry of range difference location”, IEEE Transactions on Aerospace and Electronic Systems, Vol. AES-8, No.3, pp.821-835, Nov. 1972.

[30] Y. T. Chan, and K. C. Ho, “A simple and efficient estimator for hyperbolic location”, IEEE Transactions on Signal Processing, Vol. 42, No. 8, pp.1905-1915, Aug. 1994.

[31] B.T. Fang, “Simple Solution for Hyperbolic and Related Position Fixes”, IEEE Transactions on Aerospace and Electronic Systems, Vol.26, No. 25, pp.748-753, 1990.

[32] H. C. Schau and A. Z Robinson, “Passive source localization employing intersecting spherical surfaces from time-of-arrival differences”, IEEE Transactions on Acoustics, Speech, and Signal Processing, Vol. ASSP-35, No. 8, pp.1223-1225, Aug. 1987.

[33] J. O. Smith and J. S. Abel, “Closed-form least-squares source location estimation from range-difference measurements”, IEEE Transactions on Acoustics, Speech, and Signal Processing, Vol. ASSP-35, No. 12, pp.1661-1669, Dec. 1987.

[34] H. Elkamchouchi and M.A.E. Mofeed, “Direction-of-Arrival Methods (DOA) and Time Difference of Arrival (TDOA) Position Location Technique”, IEEE Radio Science Conference, Cairo, Proceedings of the Twenty-Second National, pp.173-182, March 2005.

[35] M.I. Skolnik, “Intoduction to radar Systems”, 3rd Ed., New York, McGraw Hill, 2001, Chapter 2; Chapter 7, pp. 49-65.; 403-423.

[36] N. J. Willis, H.D. Griffiths, “Advances in Bistatic Radar”, Raleigh, SciTech, 2007, Chapter 9, pp. 230-317.

[37] F.E. Nathason, J.P. Reilly and M.N. Cohen, “Radar Design Principles”, Raleigh, SciTech, 1999, Chapter 5, pp.208.

[38] Sikorsky SH-60B/F Seahawk Basic Avionics Maintenance Review Course; class materials, 1995.

APPENDIX

Data Table of Generalized Mean Bistatic Scattering Coefficients of Different Natural Terrains

Cited	Band	Pol.	σ° (dB)	ϕ	θ_i	θ_r	ß	Terrain	Year
[4]	S	VV	-36,5	20°-70°	-	-	≤1°	Foliated Tree	1994
		HH	-42,5					Foliated Tree	
		VV	-34,9					Defoliated Tree	
		HH	-39,1					Defoliated Tree	
[5]	S	VH	-46,1	20°-70°	-	-	≤1°	Foliated Tree	1995
		HV	-46,7						
[6]	S	VV	-39,3	25°-75°	-	-	≤1°	Foliated Tree	1995
		HH	-44,1						
		VH	-47,3						
		HV	-47,9						
[7]	S	VV	-28,3	25°-65°	-	-	≤1°	Defoliated Tree	1997
		HV	-38,5						
		HH	-33,1						
		VH	-34,7						
[8]	S	VV	-27,1	35°-85°	-	-	0,5°≤β ≤2,0°	Foliated Tree	2001
[9]	X	HH	-21,4	0°-140°	60°	60°	-	Sand (smooth)	1965
			-26,7		70°	70°			
			-23,2		80°	80°			
			-29,4		85°	85°			
			-18,2		60°	60°		Loam	
			-15,9		70°	70°			
			-20		80°	80°			
			-20,7		85°	85°			
			-15,4		60°	60°		Soybean Foliage	
			-18,3		70°	70°			
			-23,1		80°	80°			
			31,9		85°	85°			
		HV	-20,5		60°	60°		Sand(smooth)	
			-19,7		60°	60°		Soybean Foliage	
		VV	-26		70°	70°		Sand(smooth)	
			-14,7					Loam	
			-15,9					Soybean Foliage	

[9]	X	HH	-9,6	0°	20°	-80°-80°	-	Sand(smooth)	1965
			-12,4		40°				
			-12		65°				
			-11,3		70°				
			-15,2		75°				
			-16,3		80°				
			-3,9		20°			Sand(rough)	
			-5,8		40°				
			-12,2		75°				
			-10,8		80°				
			-7,6		20°			Dry Grass	
			-9,5		40°				
			-14		75°				
			-14,2		80°				
			-6,4		20°			Loam	
			-9,1		40°				
			-12,8		65°				
			-8,4		70°				
			-8,5		40°			Loam with Stubbl	
			-2,6		40°			Soybean Foliage	
		VV	-12,8		20°			Sand(smooth)	
			-16,7		40°				
			-13,3		70°				
			-21		75°				
			-19		80°				
			-6,5		20°			Sand(rough)	
			-12,8		40°				
			-18,6		75°				
			-15,5		80°				
			-11,2		20°			Dry Grass	
			-12,8		40°				
			-19,5		75°				
			-17,2		80°				
			-10,5		20°			Loam	
			-15,3		40°				
			-13,8		70°				
			-17,4		80°				
			-12,4		40°			Loam with Stubble	
			-17		40°			Soybean Foliage	
		VV	-26,5	0°-140°	60°	60°		Sand(smooth)	
		HH	-17,6						
		VH	-21,2						
		VV	-24,9		70°	70°			

[9]	X	HH	-27,4	0°-140°	70°	70°	-	Sand(smooth)	1965
		VH	-27,1						
		VV	-28,6		80°	80°			
		HH	-23,6						
		VH	-34						
		VV	-32,4		85°	85°			
		HH	-30,1						
		VV	-15,4		60°	60°		Loam	
		HH	-18,6						
		VV	-15,6		70°	70°			
		HH	-17,1						
		VV	-21,7		80°	80°			
		HH	-20,3						
		VH	-28,3						
		VV	-23,5		85°	85°			
		HH	-20,8						
		VH	-24,4						
		VV	-13,5		60°	60°		Soybean Foliage	
		HH	-17,3						
		VH	-20,1						
		VV	-29,3		80°	80°			
		HH	-23,6						
		VV	-13,2	0°	20°	-80°-80°		Sand(smooth)	
		HH	-10						
		VH	-20,9						
		VV	-16,4		40°				
		HH	-6,9						
		VH	-10,8						
		VV	-17,2		70°				
		HH	-10,5						
		VV	-21,7		75°				
		HH	-16,5						
		VV	-11,3		20°			Loam	
		HH	-6,8						
		VH	-19,7						
		VV	-15		40°				
		HH	-9,3						
		VH	-23,4						
		VV	-20,7		75°				
		HH	-11,7						
		VV	-8		20°			Loam with Stubble	
		HH	-9,4						
		VH	-21,7						
		VV	-12,2		40°				
		HH	-7,4						

		VH	-20,9		40°			
		VV	-13,1					
		HH	-11,6		65°			
		VH	-27,2					
		VV	-16,8					
		HH	-10,7		70°			Loam with Stubble
		VH	-31,1					
		VV	-19					
		HH	-13,7		75°			
		VH	-30,7	0°		-80°-80°		
		VV	-17					
		HH	-10,5		80°			
		VH	-21,6					
		VV	-15,6					
		HH	-11		85°			
		VH	-25,1					
		VV	-9,5					
		HH	-6,5		20°			
		VH	-19,5					
		VV	-12,2					
		HH	-9,4		40°			
		VH	-19,9				-	Dry Grass
		VV	-17,4					
		HH	-13,1		80°			
		VH	-22,4					
		VV	-16,1					
		HH	-14,6		85°			
		VH	-21,4					
		VV	-8,9					
		HH	-5,2		20°			
		VH	-15,6					Soybean Foliage
		VV	-15,5					
		HH	-0,8		40°			
		VH	-10,5					
		VV	-5,4					
		HH	-3,3		20°			
		VH	-22,4					
		VV	-8,5					
		HH	-5,6		40°			Sand(rough)
		VH	-22,3					
		VV	-16,7					
		HH	-10,2		80°			
		VH	-25,5					

		VV	-26,9	0°-140°	60°	60°		Sand(smooth)	
			-29		80°	80°			
		HH	-21,7		60°	60°			
			-24,9		80°	80°			
		VV	-14,9		60°	60°		Loam	
			-22,6		80°	80°			
		HH	-18,3		60°	60°			
			-19,2		80°	80°			
		VV	-13,8		60°	60°		Soybean Foliage	
			-28,4		80°	80°			
		HH	-17,1		60°	60°			
			-25,1		80°	80°			
[10]	Ka	VV	-3,6	-	-	-	15°-45°	Sand	2002
			-12,7					Gravel	
			-17,1					Sod	
	Ku		-2,7					Sand	
			-9,4					Gravel	
			-16,9					Sod	
	X		-2,6					Sand	
			-5,5					Gravel	
			-15,4					Sod	
[11]	X	VV	-18,9	-	45°	-40°-70°	-	Bare Sand Surface	1991
		HH	-13,8						
		HV	-25						
		VV	-11,8					Sand Surface with Pine Litter Layer	
		HH	-8,3						
		VH	-19,8						
[12,13]	X	HH	-7,6	0°-180°	75°	80°	-	Tall Weeds and Scrub Trees; Dry	1978
	L		-14,6						
	X		-10,5		70°				
	L		-16,4						
	X		-10,8		80°				
	L		-16,2						
	X	HV	-10,2		75°				
	L		-18,6						
	X	HH	-13,6	0°-105°	80°	85°		Flat Grass and Cement Taxiway; Dry	
	L		-18,8						
[14]	L	HH	-23,4	0°-180°	60°	80°	-	Tree-Orchard on Wet Ground with 6 inch Snow Covered	1979
		HV	-31,3						
	X	HH	-18,4						
		HV	-20,4						
	L	HH	-30,4		70°				
		HV	-38,4						

[15]	L	HH	-15,7	0°-180°	45°	45°	-	Spruce (dense)	2005
		VH	-20,4						
		HH	-5,4					Spruce (sparse)	
		VH	-16,3						
		VV	-27,2	120°	30°	10°-70°	-	Aspen	
		HH	-27						
		VH	-28,6						
	X	VV	-24,2						
		HH	-17,9						
		VH	-17,9						
	C	VV	-20						
		VH	-20,8						
[16]	L	HH	-13,9	0°-180°	25°	25°	-	Corn	2006
		HV	-14,9						
		HH	-18,4					Soil	
		HV	-20,9						
[19]	Ka	VV	-14,3	0°-180°	66°	66°	-	Sand (smooth)	1988
		HH	-16,3						
		HH	-11		60°	60°			
		HV	-17,4						
		HH	-11,6					Rough (sand)	
		HV	-17,3						
		HH	-6,7					Gravel	
		HV	-8,6						
[20]	Ka	VV	-7,9	0°	20°	0°-70°	-	Soil (rough)	2003
		HH	-6,6						
		HV	-14,7						
		VH	-14,3						
[21,22]	X	VV	-	0°-180°	0°-90°		-	Forest, rural land and semi desert	1967
		HH							
[23]	X	VV	-	0°	Low graz. Angle		≈180°	Beach and sand dunes	1979